SYNTHESIS AND CHARACTERIZATION OF CdS_xSe_{1-x}/ZnS ALLOY CORE/SHELL NANOCRYSTALS: PHOTOLUMINESCENCE QUANTUM YIELD IMPROVEMENT WITH INFLUENCE OF COMPOSITION

By

Jessica Annette Sammons

Thesis

Submitted to the Faculty of the

Graduate School of Vanderbilt University

in partial fulfillment of the requirements

for the degree of

MASTER OF SCIENCE

in

Chemistry

August, 2009

Nashville, Tennessee

Approved:

Sandra J. Rosenthal, Ph.D.

Timothy P. Hanusa, Ph.D.

ACKNOWLEDGEMENTS

I would like to thank the following people:

My advisor, Dr. Sandra J. Rosenthal, for the allowing me the opportunity to conduct research on this project.

Professors Charles Lukehart, Timothy Hanusa and Bridget Rogers, for their additional help and support.

Professor Anthony B. Hmelo, for training and guidance with the Rutherford Backscattering experiment.

Albert Dukes III, for the providing me the idea of shelling alloy nanocrystals.

All members of the Rosenthal research group, especially Dr. Nathaniel Smith, Dr. James McBride, Albert Dukes, Michael Schrueder, Jerry Chang, Becky Ordnoff, and M. Danielle Garrett for their help, advise, and friendship.

Funding for this work was provided by several Teaching Assistantships from Vanderbilt University and grants from the Department of Energy.

TABLE OF CONTENTS

LIST OF FIGURES

CHAPTER I

INTRODUCTION

1.1 Overview

Semiconductor nanocrystals have been the focus of extensive research because of their unique size-dependent optical and electronic properties,[1-3] which are of great fundamental and applied interest. Various applications, such as light-emitting diodes (LEDs),[4-7] photovoltaics,[8, 9] single-electron resistors,[10, 11] and fluorescent tags for biological imaging.[12-14], already utilize the size tunable properties that result from the quantum confinement of the exciton within the core. A variation on the idea of binary semiconductor nanocrystals, alloy nanocrystals (AB_xC_{1-x}) are not only size tunable but also compositionally tunable materials (Figure 1.1) allowing for continuous control of their physical and optical

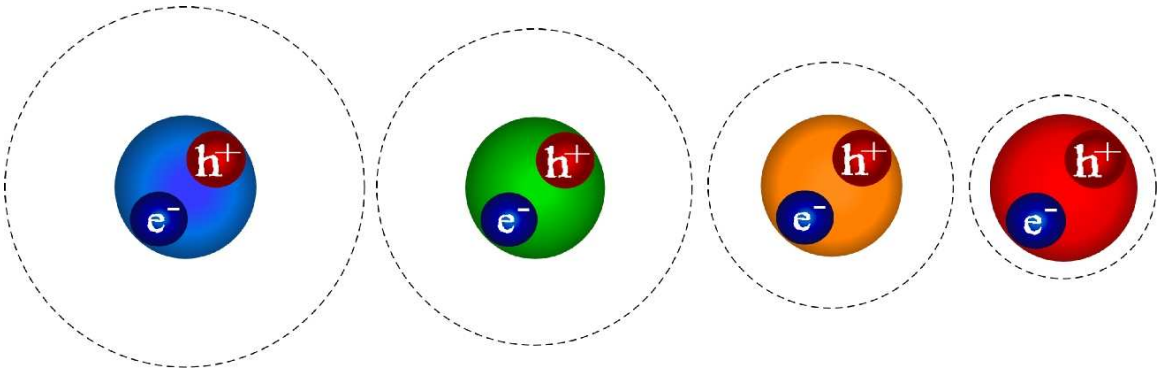

Figure 1.1. Illustration of quantum confinement in CdS_xSe_{1-x} nanocrystals. The dotted line represents the Bulk Bohr diameter, which decreases as the value of the variable *x* decreases. As the band gap energy decreases, the fluorescence of nanocrystals of similar size is seen to shift towards the red.

properties with the increase in the value of the variable x.[15] The change in nanocrystal constitution results in the extension of the exciton energy in the band gap of the nanocrystal, allowing researchers to synthesize size and color tunable nanocrystals which have the ability to access to wavelengths that are difficult to achieve with binary compounds. Alloy nanocrystals may be the solution for applications with dual requirements, requiring small nanocrystals in varying colors, such as *in vivo* imagining, multiplexing experiments[16] or photovoltaic applications.[17] To date, several II-VI semiconductor alloy nanocrystals have been synthesized: CdS_xSe_{1-x},[15] $Cd_xZn_{1-x}S$,[18] $Cd_xZn_{1-x}Se$,[19, 20] $CdSe_xTe_{1-x}$,[21] CdS_xTe_{1-x}[22] and $HgSe_xS_{1-x}$.[23]

Lattice mismatch of the two components of the psuedobinary compound results in a homogeneously alloyed nanocrystals that suffer from low fluorescence quantum yield. This presents a problem for implementation and applications. An inspired solution to the problem of low quantum yield was first reported for semiconductor nanocrystals by Hines and Guyot-Sionnest.[24] Nanocrystal cores are encapsulated by a wider band gap semiconductor material confining electron and hole recombination to the core, eliminating fluorescence quenching surface trap states. This process of shelling nanocrystal cores can be extended to shelling alloy nanocrystal cores, and would prove useful in the production of high quantum yield nanocrystals for use in future applications.

In order to increase the efficiency of the CdS_xSe_{1-x} nanocrystals and investigate the effect of composition on photoluminescence quantum yield, this research has examined the shelling of alloy nanocrystals of similar size and varying compositions with a wider band gap material, ZnS. To date, there have been no reports of shelled homogeneous semiconductor

alloy nanocrystals (AB_xC_{1-x}). In addition to this, once the alloy nanocrystals have been modified, there is a possibility of further functionalization for biological applications.

1.2 Quantum Confinement in Semiconductor Nanocrystals

Semiconductor nanocrystals' optical and electronic properties are a result of the quantum confinement of their photocreated electron-hole pairs. In bulk semiconductors, when excited, an electron separates from the hole at a characteristic distance known as the bulk Bohr radius. As the size of the crystal decreases below the bulk Bohr radius, the energy of the first excited state increases, and the nanocrystal qualitatively follows particle-in-a-box behavior.[25]

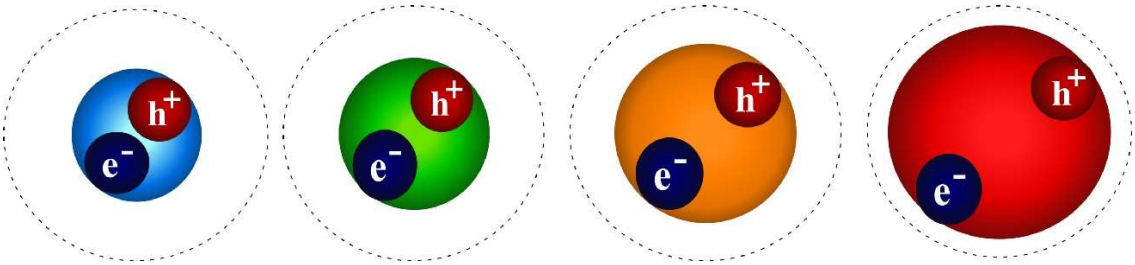

Figure 1.2. Illustration of quantum confinement in CdSe nanocrystals. The dotted line represents the Bulk Bohr diameter. As the size of the nanocrystal increases, the band gap energy decreases and the fluorescence shifts towards the red.

The energy difference between the valence and conduction band can be estimated to the first approximation as:

$$E_{ex} = \frac{h^2}{8R^2}\left(\frac{1}{m_e}+\frac{1}{m_h}\right) - \frac{1.8e^2}{4\pi\varepsilon_{CdSe}\varepsilon_0 R} + \frac{e^2}{R}\overline{\sum_{k=1}^{\infty}\alpha_k\left(\frac{S}{R}\right)^{2k}} \qquad (1.1)$$

where *h* is Plank's constant, *m* is mass, and *R* is the nanocrystal radius, accounting for kinetic, coulombic, and polarization energies of the electron and hole.[26] The inverse square relationship between energy and nanocrystal radius explains why as the nanocrystal increases in size, the band gap narrows and shifts fluorescence toward redder wavelengths. In an ideal system the energy of the photon absorbed by the nanocrystal would be equal to the energy of the photon emitted in radiative recombination; however, energy is lost in nonradiative processes resulting mainly from unpassivated surface atoms that act as hole traps,[1] and lattice strain from defect sites. The efficiency of radiative electron and hole recombination is measured by quantum yield photoluminescence.

1.3 Shelling

For many applications it is desirable to produce nanocrystals with high luminescence quantum yield. The quantum yield of pyrolytically synthesized CdSe is about 10% at room temperature. [27] Shelling is a very useful surface modification method which drastically improves fluorescence by growing a heteroepitaxial layer of a wide band gap semiconductor material around a core nanocrystal, confining the electron and hole recombination to the core and eliminating fluorescence quenching from surface trap states. In the case of CdSe nanocrystals, ZnS is most commonly used to create CdSe/ZnS core/shells which exhibit up to a 60% quantum yield.[24] Indeed, core/shells of CdSe/CdS/ZnS have been created that can exhibit a quantum yield of nearly 100%.[28] In addition to improved photoluminescence, shelling nanocrystals with a wider band gap material also enhances electroluminescence and stability against photo-oxidation.[24] It also acts as an encapsulant, creating a more robust

particle containing toxic elements such as cadmium, and allowing for surface modification for further functionalization for use in biological applications.

1.4 CdS_xSe_{1-x} Alloys

Alloys are characterized by their combination of two or more metals, semiconductors, or insulators, having properties differing from that of the composite pure materials. CdS_xSe_{1-x} is a type of alloy that is known as psuedobinary, because it is composed of two compound semiconductors, CdS and CdSe. In the same way that binary semiconductors properties change as crystal sizes reach the nanometer scale, semiconductor alloy nanocrystals allow for continuous tunability of their physical and optical properties through variations of the ratios of transition metals and/or chalcogens. This allows an added degree of freedom in tuning the nanocrystal's properties, independent of their size, and extends the properties to that of each characteristic binary compound and beyond. Nanocrystals that have varied amounts of two transition metals have properties that change in a somewhat linear fashion with their composition, while nanocrystals with varied amounts of two chalcogens (e.g. CdS_xSe_{1-x}) sometimes have a more nonlinear dependence on the ratio, and their properties can be more difficult to predict. Bernard and Zunger[29] explained these nonlinear effects, or "optical bowing," by the structural and electronic effects of different atomic sizes, electronegativities, and lattice constants of the ions involved in the semiconductor compounds. The lattice constant, a, of CdS_xSe_{1-x} is seen to vary linearly with composition.[30]

$$a(x) = xa_{CdS} + (1-x)a_{CdSe} \tag{1.2}$$

Meanwhile other physical properties of CdS_xSe_{1-x} alloys, such as band gap, vary nonlinearly:

$$E_g(CdS_xSe_{1-x}) = xE_g(CdS) + (1-x)E_g(CdSe) - bx(1-x) \tag{1.3}$$

and the bowing constant, *b*, describes the degree of nonlinearity. Nanocrystals are characterized by their quantum confinement, and so in addition to composition, size dependence of the bandgap must be considered[26] and when combined[15] gives:

$$E_g(x,d) = E_g(x,\infty) + \frac{a_x}{d} + \frac{c_x}{d^2} \tag{1.4}$$

where *d* is the diameter of the nanocrystal (Å), and *a* and *c* are the linear combinations of the binary constituents.

$$\begin{aligned} a_x &= xa_1 + (1-x)a_2 \\ c_x &= xc_1 + (1-x)c_2 \end{aligned} \tag{1.5}$$

Swafford *et al.*[15] successfully synthesized CdS_xSe_{1-x} nanocrystals, investigated their homogeneity and optical properties, and confirmed the tunability of the alloy nanocrystals by size and composition. They also explored the composition dependence of the Stoke's shift, which changed due to nonlinear effects. Rutherford backscattering spectroscopy was used to investigate the homogeneity as well as the composition of the alloy nanocrystals. Because the synthesized alloys do not always have the same ratios as the original precursor mixtures, RBS proved to be an effective method for determining the alloy stoichiometry.

Garrett *et al.*[31] investigated the carrier dynamics and the effect of surface trap states of these CdS_xSe_{1-x} alloy nanocrystals using ultrafast fluorescence upconversion spectroscopy showing the size and composition dependent fluorescence lifetimes at the band edge which result from the change in availability of surface trap sites and sulfur concentration.

1.5 Concluding Remarks

In this chapter, we have reviewed the basic properties of semiconductor nanocrystals, resulting from quantum confinement, and the added degree of freedom available in alloy nanocrystals. Shelling offers the ability to dramatically increase the fluorescence quantum yield of conventional binary nanocrystals, and thus should be explored for improving the quantum yield of alloy nanocrystals. In the following chapters, the synthesis of CdS_xSe_{1-x}/ZnS core/shells and their analysis by UV-Vis absorption spectroscopy, fluorescence spectroscopy, RBS, and TEM to determine their size, composition, and shelling will be described. This work is the first example of the intentional shelling of homogeneous alloy nanocrystals. On a practical level, this opens doors for future applications by allowing further surface functionalization of nanocrystals with higher quantum yields. On a fundamental level, this shelling will allow further insight into origin of the optical properties of the alloy nanocrystals.

CHAPTER II

EXPERIMENTAL

2.1 CdS_xSe_{1-x} Alloy Synthesis

The method of synthesizing CdS_xSe_{1-x} is discussed below in detail and was previously described by Swafford *et al.*[15] The cadmium source most commonly used in early binary CdX (X= S, Se, Te) synthesis was dimethylcadmium, $Cd(CH_3)_2$, which is an expensive, air-sensitive, toxic, pyrophoric chemical. To convert to a "greener" cadmium source, CdO has replaced dimethylcadmium as a safer and cheaper alternative, while still producing nanocrystals of good quality. In contrast to prevailing binary synthetic methods which use the pyrolysis of organometallic precursors in trioctylphosphine oxide (TOPO) and phosphonic acid,[27, 32, 33] the alloy synthesis is a variation of the synthesis of Yu *et al.*[34] which uses oleic acid (OA) to form a Cd-oleate complex with the CdO precursor in a non-coordinating solvent, octadecene (ODE). Nanocrystals synthesized by this method are coated with OA as the surface ligand, and are generally of a poorer quality and have a larger size distribution because nucleation and growth is more rapid and less controlled. However, this synthetic technique allows for the formation of CdS, CdS_xSe_{1-x}, and CdSe and is therefore employed for alloy synthesis.

2.1.1 CdSe, CdS, and CdS_xSe_{1-x} Synthesis

Cadmium oxide (Puratrem, CdO, 99.999%), oleic acid (OA, 90%) 1-octadecene (ODE, 90%), tri-*n*-butylphosphine (TBP, tech grade 97-99%), selenium shot (200 mesh),

sulfur powder (Fisher, reagent grade), hexanes, toluene, butanol, ethanol, acetone, and chloroform (all reagent grade), were purchased from Sigma-Aldrich or Strem if not otherwise indicated and used as delivered. The cadmium precursor was prepared by combining 0.256 g of CdO, 2.4 mL OA and 10 mL of ODE in a 100 mL three neck round-bottom flask fitted with a temperature probe, bump trap, and a rubber septum. The reaction mixture was stirred and purged with argon until the reaction reached 140 °C. The temperature was then raised to 310 °C and stirred until the solution became clear and colorless. For CdS_xSe_{1-x} alloy nanocrystals, when the temperature reached 310 °C, an injection solution of 10*x* mL of 0.1 M S:ODE with 10(1-*x*) mL of 0.1 M Se:TBP:ODE (diluted with ODE from a 4 M Se:TBP stock solution, where x is less than 1) was swiftly injected and the temperature was reduced to 275 °C. Nanocrystals will not grow larger than approximately 36 Å in diameter without the addition of growth solution. Aliquots were taken and diluted with toluene for subsequent characterization. Post-synthesis isolation of the nanocrystals was carried out by precipitation in a butanol:ethanol (1:4) mix and collected by centrifugation. The pelleted solid was dispersed in 5 mL of chloroform and the nanocrystals precipitated by the addition of acetone and collected by centrifugation.[35] The pelleted solid containing the nanocrystals were once again precipitated with the chloroform:acetone mix and collected by centrifugation. The cleaned alloy nanocrystals were dispersed in hexanes for characterization. Some analysis required cleaner nanocrystals, in which case the nanocrystals dispersed in hexanes were precipitated out of solution by a butanol:ethanol (1:4) mix and collected by centrifugation. This process was repeated as many as six times.

2.2 Core/Shell Synthesis

Even high quality, well made CdSe nanocrystals have a very low quantum yield, ranging from 0-15%, yet many applications demand the high luminescence quantum yield. Hines and Guyot-Sionnest were the first discover that the luminescence of such semiconductor nanocrystals can be greatly improved by growing a heteroepitaxial layer of a wider band gap material on a nanocrystal core.[24] The first core/shells were made by growing a layer of ZnS around CdSe cores, which improved the quantum yield of the material from 10% to 50%. The shelling layer passivates surface trap states and confines exciton recombination to the core, resulting in more efficient radiative recombination. Recently, advances have been made producing materials with near unity quantum yield.[28] The original synthesis used a Zn/S/TOP stock solution which used dimethylzinc($ZnMe_2$) and bis(trimethylsilyl)sulfide [$(TMS)_2S$] as the zinc and sulfur precursors, dissolved in trioctylphosphine, TOP. In the same manner as the original nanocrystal methodologies, the shelling procedures have been refined to exclude air sensitive chemicals and aim for a greener and more cost effective synthesis.

2.2.1 CdS_xSe_{1-x}/ZnS Core/Shell Synthesis.

Shelling of the alloy nanocrystals was carried out following the procedure reported by Riess *et al.*[36] with modifications. A sample of purified nanocrystals in hexanes, 20 mL of ODE and 6 mL of OA were combined in a 100 mL three-neck flask fitted with temperature probe, short-path distillation apparatus, and rubber septum. The mixture is heated under argon with stirring to 200 °C, distilling off the hexanes. When the temperature reached

200 °C, a solution consisting of equal volumes of 0.1M zinc napthonate:toluene, 0.1M S:di-butyl ether, and toluene were mixed in a syringe. The ZnS solution was pumped at a constant rate of 0.78 mL/min into the nanocrystal solution and aliquots were taken at regular time intervals. The absorption and fluorescence measurements were monitored and addition of the shelling solution was stopped when the fluorescence ceased to increase. Isolation of the shelled alloy nanocrystals was carried out in the same manner as the alloy nanocrystals.

2.3 Characterization

Once the nanocrystals had been synthesized and cleaned they were characterized to determine size, monodispersity, quantum yield, shape, and structure. Static absorption was used to analyze the band gap energy and correspondingly the size of the nanocrystal sample (Section 2.3.1). Static Emission was used to determine the monodispersity of the nanocrystal sample, as indicated by the full width at half-maximum (FWHM), as well as the fluorescence quantum yield (Section 2.3.2). Transmission electron microscopy was used to determine the size and size distribution, as well as reveal insight as to the crystallinity of the nanocrystal sample (Section 2.3.3). Lastly, Rutherford backscattering spectroscopy was used to determine the elemental composition (Section 2.4.4).

2.3.1 Static Absorption

UV-visible absorption spectroscopy is an extremely useful analytical tool for monitoring nanocrystal properties. As a result of quantum confinement in semiconductor nanocrystals, the first excitonic peak detected by static absorption can be used to determine the band-edge energy and consequently the nanocrystals size[37] and size distribution.[38]

Nanocrystal samples were placed in a 1-cm path length cuvette and diluted in either toluene or hexanes to an optical density of less than 1. Absorption spectra were collected from 300-800 nm using a Varian Cary 50 UV-vis spectrophotometer. High quality nanocrystal samples are indicated by sharper and more defined spectral features. The relationship between the band gap, as revealed by absorption, and size has been described for binary CdS and CdSe,[37] and was found to also be nonlinearly related for CdS_xSe_{1-x} alloy nanocrystals,[15] as shown in equation 1.4.

2.3.2 Static Emission and Fluorescence Quantum Yield

Fluorometry was used to collect static emission spectra, which is of particular interest in determining the monodispersity and quantum yield of the nanocrystal samples. The quantum yield is a measure of efficiency of radiative electron-hole recombination. Fluorescence quantum yields are calculated by comparing the emission from a standard laser dye to the emission from a nanocrystal sample. To prepare samples for measuring quantum yield, the optical density (OD) of both the standard and the nanocrystal sample must be set to less than 0.1 at the desired excitation wavelength via static absorption measurements. The nanocrystal quantum yield can be determined using the equation:

$$Q = Q_R \frac{I}{I_R} \frac{OD_R}{OD} \frac{n^2}{{n_R}^2} \tag{2.1}$$

Where Q is the quantum yield, I is the integrated intensity, OD is the optical density, and n is the refractive index of the solvent. The subscript R refers to the reference standard used, with

a known quantum yield. The laser dyes used were Rhodamine 6G in methanol or Coumarin 314 in ethanol depending on nanocrystal band edge.

Photoluminescence (PL) spectra were taken on an ISS PC1 photon counting spectrofluorometer using the same sample preparation as that for absorption spectra. The PL spectra were obtained with an excitation wavelength below the nanocrystal band edge wavelength, and an emission range of 15 nm above the excitation wavelength to 800 nm.

2.3.3 Transmission Electron Microscopy (TEM)

High-resolution transmission electron microscopy (TEM) uses a focused electron beam for imaging, and this technique was used on select samples to determine the size of the nanocrystals as compared to the absorption spectra, as well as their shape and lattice order. Because there is an accepted linear relationship between size and absorption for alloy CdS_xSe_{1-x},[15] TEM analysis wasn't necessary for every sample. Images were taken on a Phillips CM20 200 kV TEM. Further details on microscope operation and sample preparation are discussed in detail by McBride.[39]

2.3.4 Rutherford Backscattering Spectroscopy

Rutherford backscattering spectroscopy (RBS) is an analytical technique that uses a high energy ion beam to bombard a sample, and measures the energy difference of backscattered ions to determine the composition of the sample. RBS has been seen to determine composition of nanocrystals samples to an accuracy of better than a picomole. [40] The stoichiometry of CdS_xSe_{1-x} as measured by RBS was previously reported by Swafford,[15]

and an in depth description of theory and sample preparation and evaluation have been presented.[41]

Rutherford backscattering spectroscopy is able to detect atoms of different atomic numbers, allowing each element to be identified as well as its stoichiometry. Each particle backscatters a characteristic energy relative to the incident beam. The energy of the scattered particles of the incident beam, $\boldsymbol{E_1}$, is related to the energy of the incident beam, $\boldsymbol{E_0}$, the mass of the helium ions of the incident beam, m_1, the mass of the target nucleus, m_2, and the scattering angle of the incident beam, θ_1, by the equation:

$$E_1 = E_0\left(\frac{m_1\cos\theta_1 \pm \sqrt{m_2^2 - m_1^2(\sin\theta_1)^2}}{m_1 + m_2}\right)^2 \tag{2.2}$$

The energy of the backscattered ions is linearly related to the channel number in the RBS spectrum, and therefore the stoichiometry of the elements can be elucidated using the ratio of integrals of the peaks. The stoichiometry of the resulting sample can be calculated by the equation:

$$\frac{N_A}{N_B} = \frac{A_A}{A_B} \times \frac{\sigma_R^B(E_o,\theta)}{\sigma_R^A(E_o,\theta)} \times \frac{\left(\sigma/\sigma_R\right)_B}{\left(\sigma/\sigma_R\right)_A} \tag{2.3}$$

where the stoichiometric ratio of element A to element B, N_A/N_B, is related to the integrals of the peaks corresponding to each element, the Rutherford-pure coulomb scattering differential

cross section, $\sigma_R(E,\theta)$, and a correction factor for cross sections that deviate from Rutherford at high and low energies, σ/σ_R.

Rutherford backscattering spectrometry (RBS) was performed using a custom-built setup.[42] Nanocrystals were diluted in hexanes to an optical density of < 1.0, and dropcast on the surface of a graphite substrate (Carbone of America), wicking to remove excess solvent. Experiments were performed under a high vacuum (< 10^{-6} Torr) with a 1.8 MeV ^{4}He ion beam. Backscattered ions were detected at an angle of 176°. Spectra were analyzed according the procedure described by Feldman *et al*.[43]

CHAPTER III

RESULTS AND DISCUSSION

3.1 Introduction

Alloy nanocrystals have the potential to become the solution for biological imaging applications with dual requirements, since they have emissions tunable by size and composition.[15] In order to utilize alloys nanocrystals they must be modified to improve the quantum yield and allow for functionalization. By shelling the nanocrystals in a similar fashion to that previously employed with binary nanocrystal core/shells,[24] the alloy nanocrystal core is encapsulated in ZnS. Creating an alloy core/shell serves to improve the quantum yield of the nanocrystal while opening the possibility of further surface modification for future applications. In addition to the practical benefit of shelling alloy nanocrystals, it also allows an avenue through which to investigate the effect of composition on alloy fluorescence. Garrett *et al.* investigated the effect of alloy composition on carrier dynamics and found that with increasing sulfur concentration, CdS_xSe_{1-x} nanocrystals have a larger concentration of trap states, affecting the radiative recombination fluorescence lifetimes.[44] In addition to fluorescence lifetimes, this increase in trap states affects the optical properties of the alloy nanocrystals. Alloy core/shell nanocrystals may give information for differentiating between the intrinsic electron trapping properties of sulfur, and surface trapping. Sulfur's intrinsic trapping would not be affected by the shelling layer, leading to a less efficient core/shell, however shelling should passivate surface trapping, leading to a more efficient and higher quantum yield material.

3.2 Results and Discussion

Synthesis of CdS_xSe_{1-x} nanocrystals of 30 ± 5 Å of varying compositions was achieved using CdO in an OA:ODE mixture. Using the OA:ODE system instead of the TOPO:HDA system yields nanocrystals with a zinc blende crystal structure rather than wurtzite, which is essential in synthesizing the CdS_xSe_{1-x} alloy nanocrystals. This method has previously been verified, yielding monodisperse samples of homogeneously alloyed nanocrystals.[15] However, the quantum yield of the nanocrystals synthesized in this system (OA:ODE) is comparatively very low. This is likely due to surface trapping caused dangling bonds or by zinc blende stacking faults and surface defects.[35]

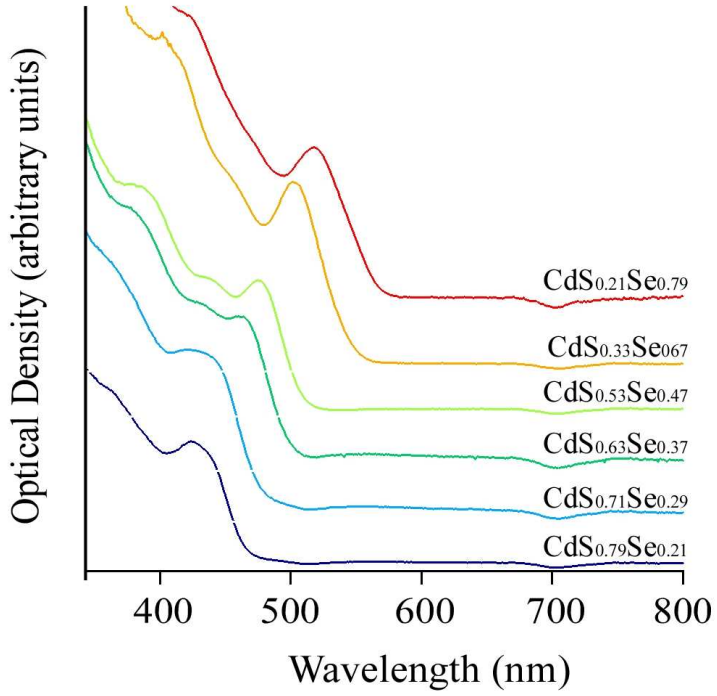

Figure 3.1. Absorption spectra of $CdS_{0.79}Se_{0.21}$ (dark blue), $CdS_{0.71}Se_{0.29}$ (light blue), $CdS_{0.63}Se_{0.37}$ (dark green), $CdS_{0.53}Se_{0.47}$ (light green), $CdS_{0.33}Se_{0.67}$ (orange), and $CdS_{0.21}Se_{0.79}$ (red) of 30 ± 5 Å.

The static absorption and emissions of the alloy nanocrystals were taken before shelling to determine size and monodispersity. From the absorption maximum, the band edge was determined and used to elucidate the nanocrystal size using equation 1.4. Absorption spectra for CdS_xSe_{1-x} nanocrystals of approximately 30 ± 5 Å are shown in Figure 3.1. Alloy nanocrystals displayed a typical band-edge emission peak, with deep-trap emission becoming more apparent as the concentration of sulfur increased, as expected with increased surface trapping. Nanocrystals with band edge emission peaks having a smooth and symmetrical line shape with a full width at half-maximum (FWHM) of 50 nm or less were considered adequately monodisperse and were used in the shelling experiments. Any change in the FWHM during shelling will reflect the focusing or defocusing of the size distributions of the alloy nanocrystals.

The need for a semiconductor with a wider band gap than both CdSe and CdS guided the choice of ZnS as the shelling material. Indeed ZnS is a popular choice and has many advantages for shelling CdS_xSe_{1-x}. A layer of ZnS can be added to core nanocrystals at a temperature that doesn't encourage core growth or ZnS nucleation. Because ZnS forms at a lower temperature than CdS, and has a 7% lattice mismatch, while the lattice mismatch for CdSe and ZnS is about 12%,[45] there is little possibility for core/shell alloying. As a shelling layer, ZnS effectively confines both electrons and holes to the core allowing for direct recombination.

The absorption and emission was monitored during the shelling process. In most cases as the shelling layer increased, the peaks in the absorption spectra did not shift a significant amount; however they did broaden, with higher energy transitions covered by the continuum of the band gap. This broadening is due to nonradiative processes, caused by

bond strain and lattice mismatch created by growth of the shell on the alloy core surface as well as a distribution of shell thickness.[46] The retention of the band edge peak in the absorption indicates that the shelling process has not allowed for core modification or core and shell alloying. The emission spectrum confirms that the quality of the nanocrystals remain intact, continually displaying a narrow band edge peak. Initially the emission peak seems to blue shift while decreasing in intensity. It is believed that the reason for this is the initial surface rearrangement that takes place as the first layer of ZnS is added. As the shelling layer thickens, the emission peak is seen to red shift only slightly, likely due to partial exciton leakage into the ZnS matrix,[46] while the intensity increases as much a five-fold. This red shifting behavior has been observed in nanocrystals allowed to grow without any shelling layer. However nanocrystal core growth is unlikely the case, during synthesis the alloy nanocrystals were allowed to grow to the largest size possible without adding growth solution, and a marked improvement in quantum yield not seen in nanocrystals grown without shelling material was observed. Indeed, a similar slight red shift has been seen in CdSe/ZnS.[24, 46] An example of the alloy emissions specta before and after completion of the shelling process is shown in Figure 3.2. The ZnS creates a heteroepitaxial layer on the surface, quenching trap sites and confining the electron and hole to the alloy core. This leads to an emission spectrum with greatly improved quantum yield, dominated by band edge recombination.

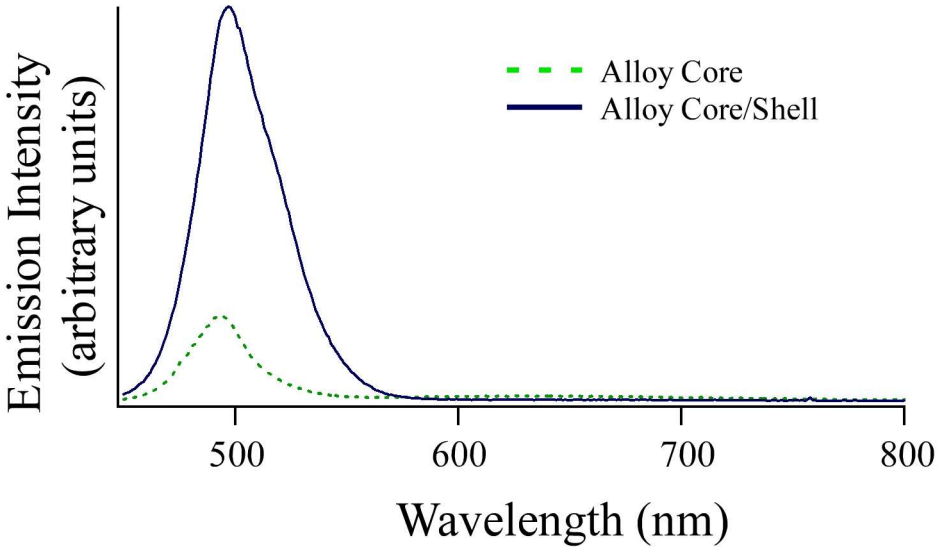

Figure 3.2. An example of the emission spectra of CdS_xSe_{1-x} before and after the shelling process. The quantum yield of this particular sample ($CdS_{0.53}Se_{0.47}$) increases from 4.8% to 22.3% with the addition of the ZnS shelling layer. There is a slight redshift of the band edge peak due to exciton leakage into the ZnS matrix.

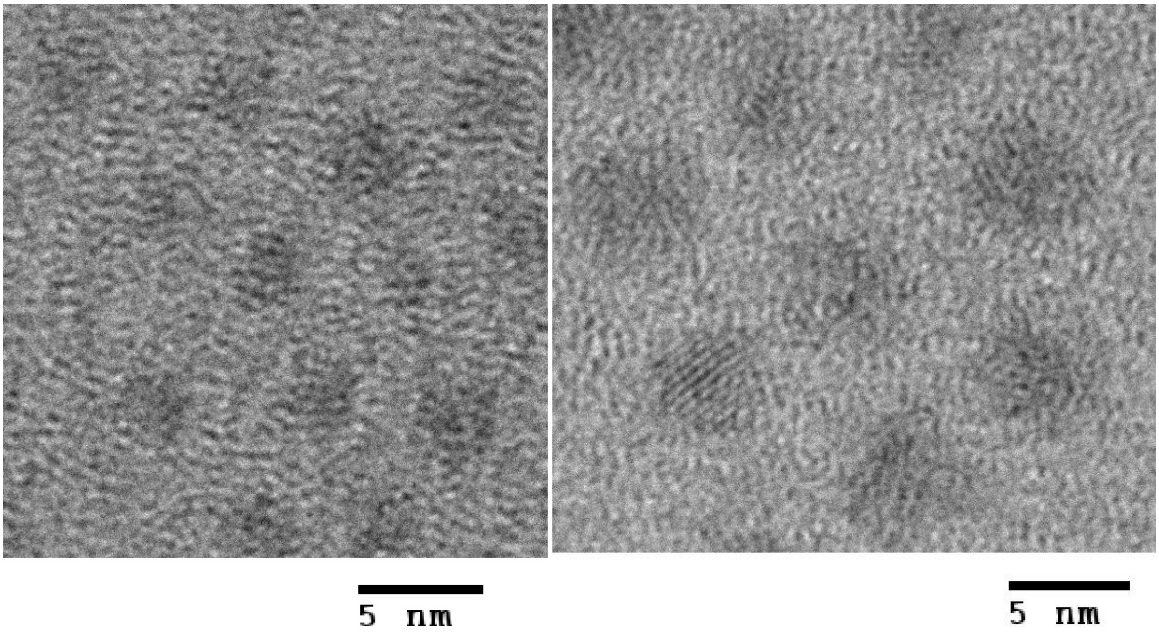

Figure 3.3. TEM image of $CdS_{0.63}Se_{0.37}$ and $CdS_{0.63}Se_{0.37}$/ZnS core/shell nanocrystals.

High resolution transmission electron microscopy images were taken to ensure that nanocrystal samples consisted of monodisperse crystals (corroborating the emission data) and to confirm the presence and thickness of a shelling layer. Figure 3.3 shows the TEM images taken before and after shelling $CdS_{0.63}Se_{0.37}$ nanocrystals. The diameter increases from about 30 Å to 50 Å, indicating a shell growth of approximately 10 Å, which corresponds to 3.2 monolayers of ZnS shell.[46] Samples imaged by TEM were seen to have a shelling layer of similar thickness.

Rutherford backscattering spectroscopy was used to determine the stoichiometry of CdS_xSe_{1-x} as well as confirm the presence of zinc for the CdS_xSe_{1-x}/ZnS core/shells. An example of normal RBS spectra before and after shelling can be seen in Figure 3.4.

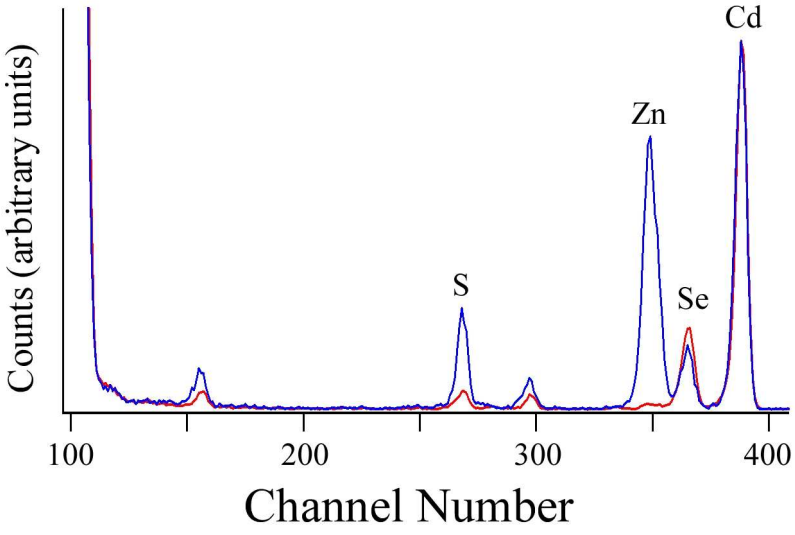

Figure 3.4. Typical RBS spectra of CdS_xSe_{1-x} (red) and CdS_xSe_{1-x}/ZnS (blue) normalized to the Cd peak. The appearance of a Zn peak and increase in the S peak qualitatively confirms shell growth. Peaks at 160 and 299 are from Oxygen, which is present on the nanocrystal surface, and Calcium, which is an impurity in the solvents used to purify the nanocrystals.

Because of reaction conditions, the stoichiometry of the synthesized nanocrystals differs slightly from the ratios used in synthesis. The true stoichiometry of the alloy

nanocrystal is calculated by equation 2.3, as determined by RBS evaluation of thoroughly cleaned samples. In addition to stoichiometry, it is also possible to calculate the average thickness of the shelling layer of the alloy core/shell.[41] Because of the different binding energies of the nanocrystal facets the shelling does not produce an even layer encapsulating the core, it is heteroepitaxial in nature, therefore the calculated shell thickness would only serve as an average estimate. The presence of a very large Zn peak as well as the increase in the S peak indicates that the expected normal shelling layer on the nanocrystal is present, but TEM serves as a better tool for quantitatively determining shell thickness.

The success of this work is seen in the enhanced fluorescence efficiency of the CdS_xSe_{1-x} alloy nanocrystals. The quantum yield was determined using a standard laser dye, matching the optical density of the nanocrystal sample and dye at a specified wavelength. In this experiment, either Rhodamine 6G in methanol or Coumarin 314 in ethanol were the preferred laser dye standards. The photoluminescence quantum yield was calculated using equation 2.1. Some general trends are detectable, as seen in Figure 3.5 which shows the quantum yield before and after shelling of various compositions.

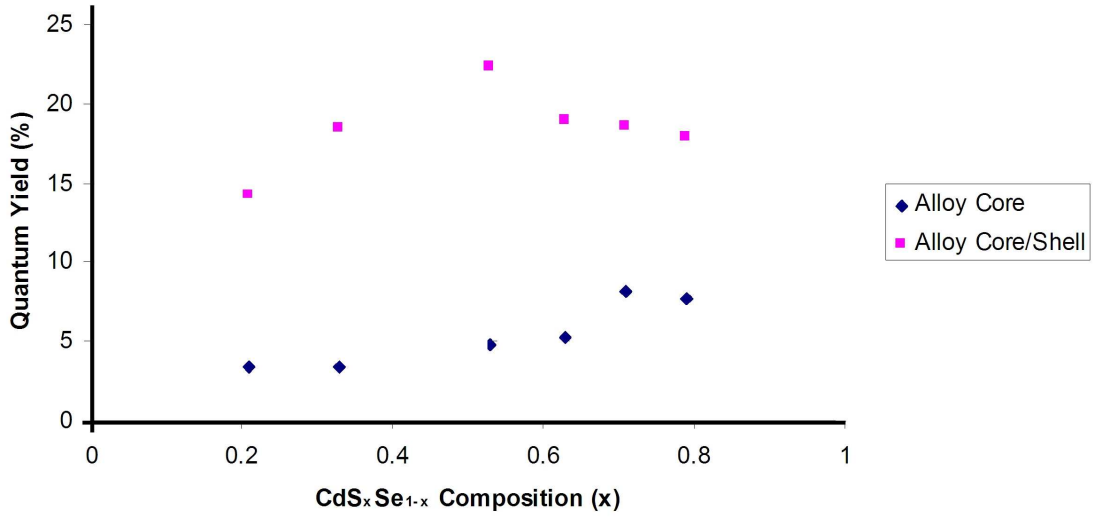

Figure 3.5. Scatter plot of quantum yield of CdS_xSe_{1-x} and CdS_xSe_{1-x} core/shells with varied values of *x*.

While the band edge emission of more sulfur heavy alloy nanocrystals is indeed less intense than selenium heavy, the effect of increased sulfur content is the increase in alloy core deep trap emission from surface trap states, contributing to an higher quantum yield overall. As the shelling layer is grown surface trap states are passivated, quenching the deep trap emission and the band edge peak is seen to dramatically increase in intensity in all samples regardless of composition. It was expected that the quantum yield of the shelled alloys would display a similarly increasing trend as seen in the alloy cores, as the lattice constant of ZnS is closer to that of CdS than CdSe resulting in less lattice mismatch. However, the quantum yield of the alloy core/shells seemed to reach a maximum at about midway through the composition. At $CdS_{0.5}Se_{0.5}$ the crystal structure has reached the maximum amount of structural disorder and has a lattice constant halfway in between CdS and CdSe, after which the surface becomes dominated by sulfur dangling bonds. The decreased improvement in quantum yield may be explained in terms of Se and S dangling

bond reactivity. Selenium dangling bonds are more reactive because of the smaller CdSe band gap, and are therefore more likely to oxidize, be bound to a ligand, and in the case of shelling, become the bond at the ZnS core/shell interface. This means that fewer Se dangling bonds will be available for hole trapping. As the concentration of S increases, so does the amount of potentially unpassivated bonds at the core/shell interface, which in conjunction with shell growth preferentially forming at the Se sites, may induce lattice strain not originally expected in comparing the lattice constants of the core and shell materials.

It has previously been seen that CdS is inherently inefficient, possessing a lower quantum yield than normal CdSe. Sulfur acts as an intrinsic electron trap, which Garrett *et al.* observed when investigating CdS_xSe_{1-x} nanocrystal fluorescence lifetimes. Shelling with a wider band gap material would be ineffective in restoring direct radiative recombination not caused by surface trap states. Trapping is seen in the shelling of more sulfur heavy alloys, the quantum yield improvement decreases with increasing sulfur content.

In any case, with the addition of a ZnS capping layer there is a dramatic increase in alloy nanocrystal quantum yield. This opens up the possibility of CdS_xSe_{1-x} use in future applications. In particular, shelling makes alloys viable possibilities for biological imaging applications by encapsulating toxic cadmium and allowing for further surface functionalization.

3.3 Conclusion

This work presents the first example of alloy semiconductor nanocrystals shelled with ZnS. The presence of the wider band gap shell formed directly on nearly monodisperse alloy cores is established by RBS and TEM. Static absorption and emission proves the retention of

the initial core size. The quantum yield of the passivated alloy nanocrystals is seen to benefit, exhibiting an unexpected trend with changing composition. In the future, these new alloy core/shell nanocrystals may be further characterized to better understand their optical properties, trends in quantum yield improvement, as well as their recombination kinetics. They may also be water-solublized and functionalized for biological imaging applications having dual requirements that would benefit from the alloy nanocrystal's added degree of freedom.

APPENDIX A

Core Modifications of CdSe Nanocrystals: Manganese Doping

Alloy semiconductor nanocrystals are compositionally tunable materials, exploiting the properties of the binary semiconductor materials that are used to create them. A different way to tune nanocrystals emission is to modify the core structure by doping with transition metal ions, introducing new energy levels into the semiconductor band structure.

Furdyna *et al.* first investigated transition metal doped bulk semiconductors, also called diluted magnetic semiconductors (DMS), and found that they exhibit optical properties tunable in respect to dopant concentration.[47] Only in the past decade has there been investigation into the doping of semiconductor nanocrystals, potentially overcoming intrinsic disadvantages such as sensitivity to thermal, chemical and photochemical disturbances, and self-absorption.[48, 49]

A.1 Manganese Doping

Among the transition metals used to dope bulk DMS, paramagnetic ions such as manganese display unique magnetic and magneto-optical properties, which result from the sp-d exchange interaction between dopant ions and semiconductor charge carriers.[50, 51] Manganese has a sharp, atomic-like emission line that is easily detectable in the visible range, making it a logical and popular choice as a dopant ion and luminescence activator.[52] In the matter of transition metal-doped II-VI nanocrystals, there have been several reports of

successful Mn^{2+} incorporation in CdS, ZnS, $Zn_xCd_{1-x}S$ and ZnSe semiconducting nanocrystals, and only a few reports of CdSe.[48, 53-61]

A.1.1 Difficulty in Manganese Doping of CdSe Nanocrystals

CdSe would be an ideal nanocrystal system to dope with Mn^{2+} because it is the most understood II-VI system and has absorption and emission within the range of visible wavelengths, making the optical properties easily detectable and useful. Manganese is isovalent to cadmium; therefore it will not contribute any extra electrons or holes, but can enhance the interaction between the charge carriers recombination by localizing the exciton before nonradiative processes can occur,[62] in turn improving the efficiency of the fluorescence. Early efforts to dope Mn^{2+} into CdSe failed to incorporate any dopant.[59] While Mn^{2+} is sufficiently soluble in bulk, it is resistant to incorporation into the CdSe nanocrystal lattice. Studies to explain the difficulty of manganese doping of CdSe have been carried out. Dalpian *et al.* proposed that the nanocrystals "self-purify," pushing out the impurities as they grow.[63] This theory assumes that nanocrystal is in thermodynamic equilibrium with its environment and that the impurity atoms are able to diffuse readily throughout the nanocrystal. However, Mn^{2+} diffusion in bulk II-VI semiconductors is negligible at liquid-phase growth temperatures, although surface diffusion may still be facile.[64] Erwin *et al.* utilized density-functional theory (DFT) to calculated the binding energies of Mn^{2+} to CdSe facets.[65] They reported that the underlying mechanism of doping is controlled by the initial adsorption of impurities onto the nanocrystal surface during growth. The efficiency of the adsorption is determined by the nanocrystals surface morphology, shape, size, and the surfactants present in growth solution. They found that theoretically,

Mn^{2+} has a high binding energy to the (001) facets of zinc blende CdSe, but no binding energy of sufficient strength to any of the wurtzite facets.

Mikulec *et al.* were the first to report a successful synthesis of Mn:CdSe[59] by organometallic decomposition using $Mn_2(\mu\text{-}SeMe)_2(CO)_8$ as a single source Mn-Se precursor. Other methods have been used to produce Mn:CdSe, such as Atomic Layer Epitaxy (ALE)[61] and the use of inorganic cluster precursors. [60] Because of the difficulty of CdSe doping, normal colloidal synthesis had not been reported until recently, when Kwak *et al.* reported a method of doping zinc blende CdSe in a paraffin oil solvent with oleic acid as the ligand,[58] which allowed ~ 4 % Mn^{2+} doping. However, only the absorption spectra and XRD were reported, which does not seem to be sufficient evidence of successful doping.

In an attempt to confirm the successful doping of CdSe with Mn^{2+} this appendix discusses static absorption and emission, Rutherford backscattering spectroscopy (RBS), high-resolution transmission electron spectroscopy (TEM), electron energy loss spectroscopy (EELS), and electron paramagnetic resonance spectroscopy (EPR) performed on nanocrystal samples synthesized by the colloidal method. The use of these analytical techniques should provide a better understanding of the extent of doping than methods previously reported.

A.2 Synthesis and Characterization of Mn:CdSe

A.2.1 Synthesis of Mn:CdSe

Cadmium oxide (Puratrem, CdO, 99.999%), cadmium acetate dihydrate ($Cd(OCOCH_3)_2{\cdot}2H_2O$, 98%), cadmium chloride ($CdCl_2$, ≥99.0%), manganese acetate ($Mn(OCOCH_3)_2$, 98%), manganese acetate tetrahydrate ($Mn(OCOCH_3)_2{\cdot}4H_2O$, ≥99.0%) oleic acid (OA, 90%) 1-octadecene (ODE, 90%), selenium shot (200 mesh), hexanes,

toluene, butanol, ethanol, acetone, and chloroform (all reagent grade), were purchased from Sigma-Aldrich or Strem if not otherwise indicated and used as delivered.

The procedure for doping CdSe nanocrystals with Mn^{2+} as submitted by Kwak *et al.* was followed[58] with modifications. A total of 2 mmol of Cd precursor (CdO, $Cd(OCOCH_3)_2 \cdot 2H_2O$, $CdCl_2$), 0.5 mmol Mn- precursor ($Mn(OCOCH_3)_2$, $Mn(OCOCH_3)_2 \cdot 4H_2O$), 10 mL ODE, and 4 mmol OA were placed in a 100 mL threeneck round-bottom flask and heated to 160°C purging with Ar until 150°C. The resulting solution was clear and colorless. When cadmium precursor was completely converted, 2.5 mmol- 3 mmol of Se precursor (Se:ODE) was injected into the hot solution and allowed to grow to the desired size. To stop growth, heat was removed and BuOH was quickly injected. Isolation of the nanocrystals was carried out by precipitation in a butanol:ethanol (1:4) mix and collected by centrifugation. The pelleted solid was dispersed in 5 mL of chloroform and the nanocrystals precipitated by the addition of acetone and collected by centrifugation.[35] The pelleted solid containing the nanocrystals were once again precipitated with the chloroform:acetone mix and collected by centrifugation after which they were subjected to further precipitation by butanol:ethanol or chloroform:acetone as many times as necessary. The clean nanocrystals were dispersed in hexanes or toluene for characterization, storage, or any other future purpose.

To create larger nanocrystals, a growth solution must be added to the cleaned nanocrystals. The solution is created by combining 0.76g of CdO, 6 mL OA, and 25 mL ODE which is then heated to 290 °C until the solution become clear and colorless. The solution was cooled to 50 °C and then 1.25 mL of 4M Se:TBP was added to the solution at

room temperature. This solution is added dropwise at a constant rate to cleaned nanocrystals in a three-neck flask at 160 °C.

A.2.2 Characterization

Once the doped nanocrystals had been synthesized and cleaned they were characterized to determine size, photoluminescence, monodispersity, shape, stoichiometry, and presence of dopant ions. Static absorption (Section 2.3.1), static emission (Section 2.3.2) transmission electron microscopy (Section 2.3.3), and Rutherford backscattering spectroscopy (Section 2.4.4) were used for the purposes expressed as discussed in the previous sections.

Scanning transmission electron microscope electron energy loss spectroscopy (STEM-EELS) is used to detect the presence of manganese in the nanocrystal samples. High resolution EELS analysis is useful for providing elemental analysis on the atomic scale. [66] Manganese is known to have a strong EELS signal, especially when in the oxidation state is +2 and it has a paramagnetic d^5 orbital arrangement.[67] However, this signal may be difficult to detect if the Mn^{2+} is not very concentrated in the nanocrystal.

Electron paramagnetic resonance (EPR), is used to measure the absorption of microwave radiation of unpaired electrons in a strong magnetic field and reveals spin interactions of bonded atoms. This allows for the detection of paramagnetic ions as well as investigation into the nature of the dopant location. The spin interactions are sensitive to the dopant's local environment, whether it is bound to the surface or incorporated into the nanocrystal.[68] Manganese (Mn^{2+}) is readily detectable by EPR because it is paramagnetic,

having five unpaired electrons occupying all five d-orbitals, giving a nuclear spin of I=5/2. Splitting patterns are predicted by the equation 2I+1.

A.3 Results and Discussion

In an attempt to synthesize Mn^{2+} doped CdSe nanocrystals by common colloidal pyrolysis method, reactions were carried out following the method of Kwak *et al.* with modifications.[58] It was found that larger nanocrystals could be synthesized using a selenium heavy reaction.

A.3.1 Early Synthesis and Preliminary Characterization

Early efforts to synthesize Mn:CdSe nanocrystals resulted in absorption spectra with two pronounced features at about 458 nm and 430 nm (Figure A1), regardless of the amount of time they were allowed to grow.

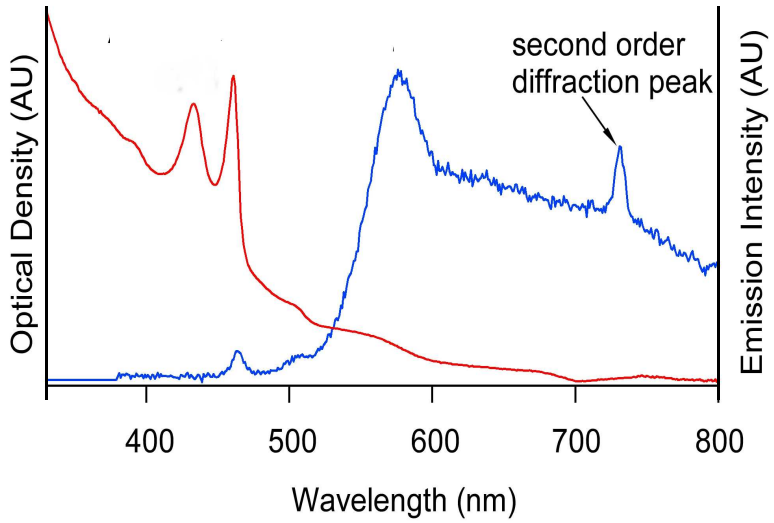

Figure A1. Typical example of normalized absorption (red) and emission (blue) spectra of early synthesis of Mn:CdSe

The sharp, two-featured absorption is unlike previously reported spectra. If these features are not characteristic of Mn:CdSe, they could possibly be the result of nanocrystal seeds occurring at energetically favorable sizes, nanocrystals with abnormal shape (i.e. rods or triangular) instead of the typical spherical shape, or of some byproduct of the reaction. If nanocrystal seeds were produced, the corresponding emission spectrum would be expected to show multiple peaks corresponding to nanocrystals of different sizes, however this does not seem to be the case. Manganese in known to have an atomic-like emission line occurring at about 580 nm, which should be observed along with band edge emission at nanocrystal sizes less than 3.3 nm.[69] Figure A1 shows the emission spectrum containing a small peak at about 467 nm, possibly the band edge peak, and a large peak at about 580 nm, indicating the presence of Mn^{2+} in the nanocrystal, followed by what appears to be deep trap emission.

The PLE spectrum collected by monitoring at 580 nm mimics the absorption spectra (Figure A2). These results have been previously observed,[69] and is believed to

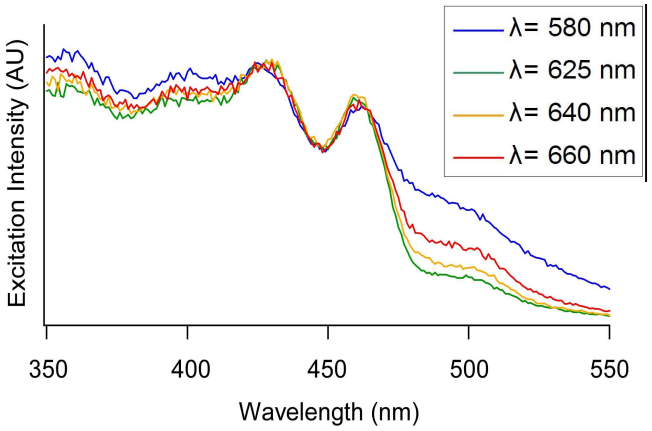

Figure A2. Normalized PLE excitation spectra monitoring at different wavelengths.

demonstrate that the Mn^{2+} emission is sensitized to the CdSe nanocrystal excitation and the exciton is quenched. Interestingly, the PLE spectra collected at 625, 640, and 660 nm, all mimic the absorption spectrum. The PLE spectrum collected by monitoring below 580 nm, such as at 467 nm (the wavelength of the taller of the two features), did not show the origin of the absorption features. If Mn^{2+} doping does the quench exciton, it is expected that the PLE collected by monitoring below the manganese transition energy would produce a featureless spectrum.

The broad emission to the red of the Mn^{2+} emission may be explained by mid gap trap sites cause by surface defects, or by bond strain or defects of the nanocrystal lattice caused by the substitution of Mn^{2+} in the crystal lattice. These lower lying levels would not be quenched by Mn^{2+} doping like band edge recombination, having recognizable deep trap behavior after 580 nm.

Preliminary RBS data determined that the nanocrystals had a detectable Mn peak. However, it is possible that if the Mn^{2+} precursor has similar solubility in solvents, the Mn detected by the RBS is in solution with the nanocrystals or loosely bound to the surface and not incorporated in the nanocrystals.

A.3.2 Early Synthesis subjected to Growth Solution

In order to create larger nanocrystals for easier imaging and test if the unusual absorption features were indicative of monodisperse doped nanocrystals seeds, or some other non-emitting material, a batch of Mn:CdSe nanocrystals was injected with a CdSe growth solution. If the nanocrystals are doped and monodisperse, it is expected that the growth solution should act as a shelling layer, encapsulating any Mn^{2+} on the surface of the

nanocrystal, and increasing the size of the nanocrystal in solution. Figure A3 shows the growth of the nanocrystals, one large peak appears in the absorption spectrum, indicative of a single size of monodisperse nanocrystals. These nanocrystals may be a result of new

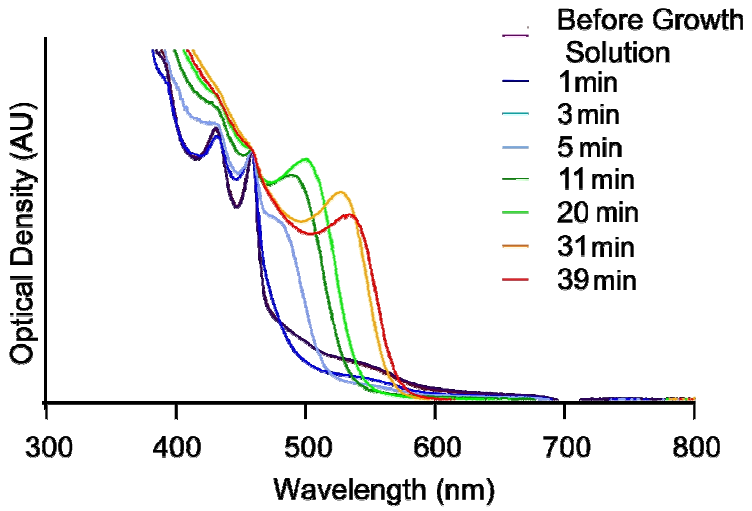

Figure A3. Normalized absorption of early synthesis of Mn:CdSe subjected to a growth solution at 160° C. Ideally CdSe would act as a shelling layer, encapsulating the impurities inside of the NC. Note that the features at 430 and 458 nm remain.

nucleation and growth, or of doped or undoped nanocrystals increasing in size. The two original absorption features become less dominant, but are still present after the growth solution has been added, however they do not move with respect to the size of the nanocrystal. Higher order energy transitions behave in the same way as the first allowed transition, as a "particle in a box,"[25] changing in energy with respect to nanocrystal size. Therefore, the peaks in the absorption spectra are indicative of some byproduct material that is not subject to quantum confinement and does not shift when subjected to a CdSe growth solution.

A.3.3 Selenium Heavy Synthesis and Characterization

A selenium heavy synthesis has been seen to increase the surface area of the 001 facet, the energetically favorable facet for doping with Mn^{2+}, in Mn:ZnSe.[65] A selenium heavy synthesis for Mn:CdSe yielded more concentrated solutions of larger nanocrystals, more quickly, and resulted in absorption spectra with one feature dependent on the growth time. Figure A4 shows an example of the absorption and emission spectra of the selenium heavy synthesis. The narrow emission peak has a full width half maximum (FWHM) of about 40 nm, indicating a fairly monodisperse sample. This band edge peak is the only feature seen in the emission spectrum because the energy of the conduction band is lower than the Mn^{2+} transition, thus dominating the emission spectrum.[69] Again it is noted that the absorption features at 430 and 458 (not pictured), believed to result from some byproduct of the reaction, are still present in the nanocrystal synthesized by the Se heavy method.

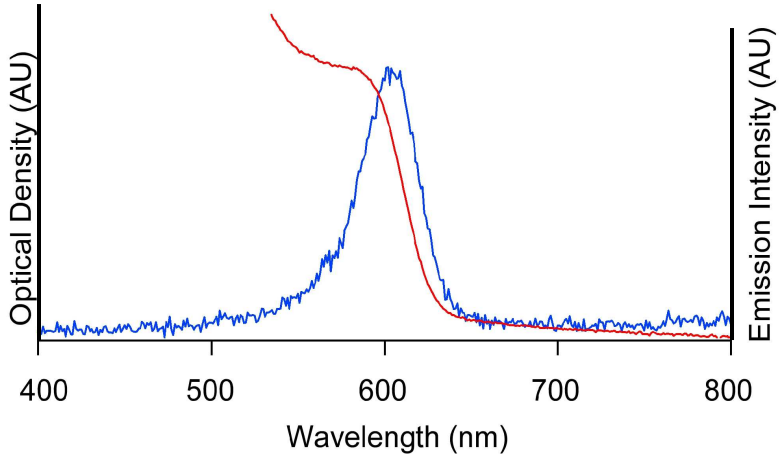

Figure A4. Typical example of normalized absorption (red) and emission (blue) spectra of selenium heavy synthesis of Mn:CdSe which yields larger NCs.

These results were more similar to what Kwak *et al.* found, and seemed quite promising. Unfortunately, since no Mn^{2+} emission can be observed, other analytical methods

must be used to evaluate the samples and provide support for successful doping. Transmission electron spectroscopy was used to image the nanocrystals and reveal their size and morphology. Rutherford backscattering spectroscopy, EELS, and EPR were used to determine if the nanocrystals were indeed being doped with Mn^{2+}, and to what extent.

A.3.3.1 RBS of Selenium Heavy Synthesis

The nanocrystals from the selenium heavy synthesis were washed multiple times and the nanocrystals as well as supernatant were evaluated using RBS (Figure A5) to determine the dopant concentration and monitor the effectiveness of the washes in

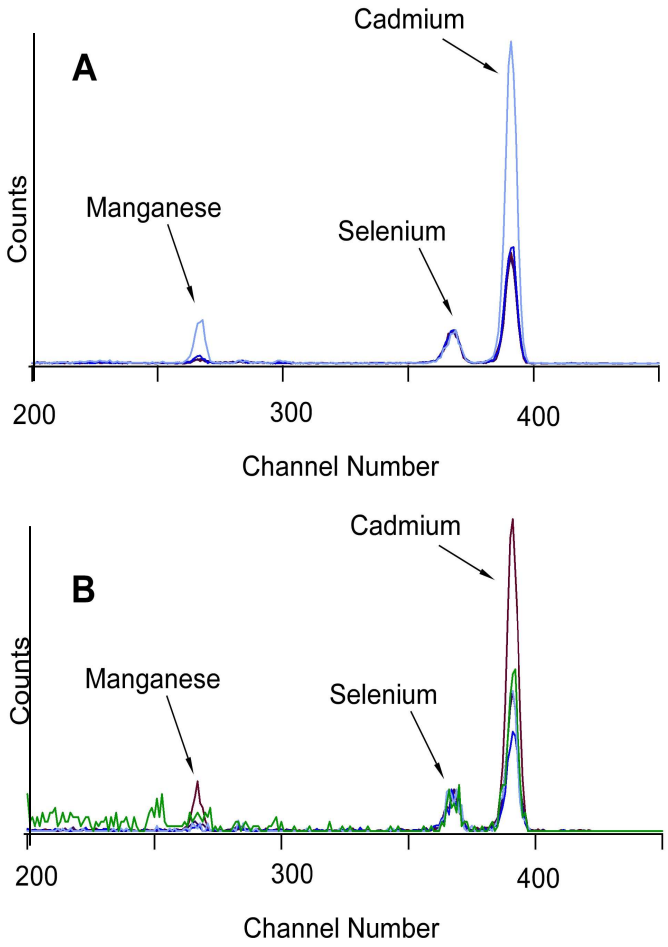

Figure A5. Normalized RBS spectrum, with regards to Se. Nanocrystals (A) and wash solution (B)

removing the Mn precursor. The nanocrystals were extracted with butanol:ethanol and additional six times after the initial purification. RBS analysis of the nanocrystals after the final wash shows a Mn signal, and the wash solution no longer shows a Mn signal, indicating the manganese being detected may be from doped Mn:CdSe.

Using equation 2.3, the stoichiometry of the Mn:CdSe was calculated. A doping range of 6.7% to 28.6% was observed, generally with less than 10% relative uncertainty. This data suggests that either the doping concentration achieved is much greater than that reported by Kwak *et al.*, or that all of the Mn is not being removed from solution, the latter being much more likely. Nevertheless, this evidence encouraged further analysis to reveal information about the location and nature of the Mn^{2+} dopant atom. The nanocrystals were evaluated by TEM, EELS and to prove the incorporation of the Mn^{2+} dopant.

A.3.3.2 TEM and EELS of Selenium Heavy Synthesis

Transmission electron microscopy (TEM) and scanning transmission electron microscope electron energy loss spectroscopy (STEM-EELS), were used to image and study the Mn:CdSe semiconductor nanocrystals. TEM is a useful technique for obtaining structural information for single nanocrystals. Figure A6 shows the TEM images of the Mn:CdSe nanocrystals from the selenium heavy synthesis. The image shows monodisperse nanocrystals with a diameter of about 5 nm.

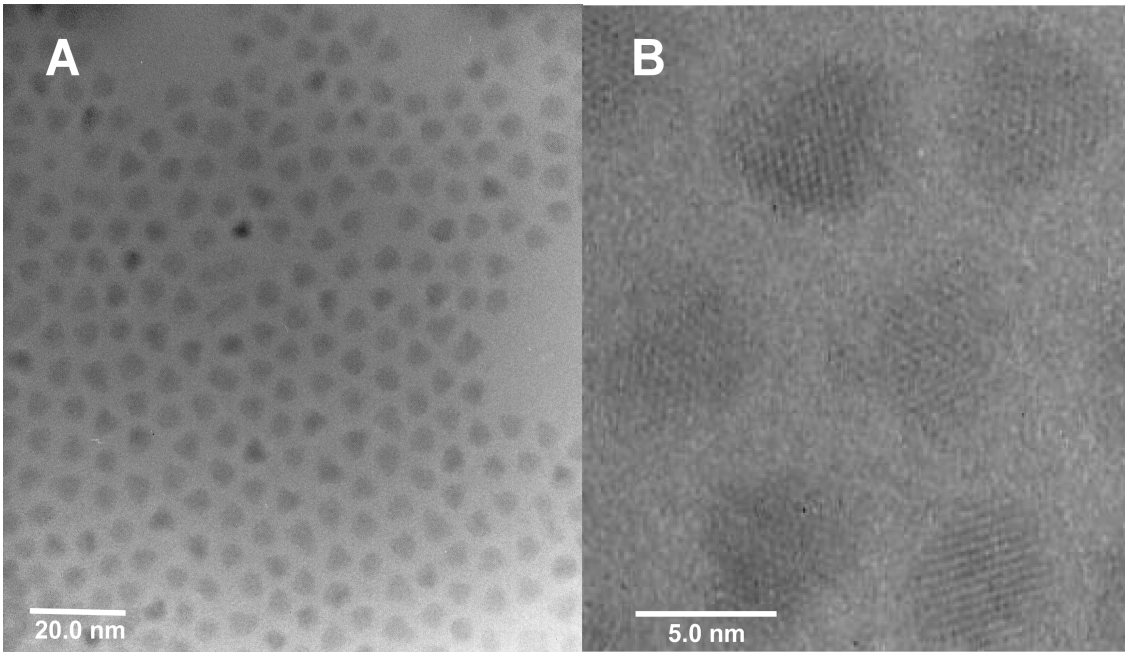

Figure A6. TEM image of Se heavy synthesis of Mn:CdSe. NCs appear fairly monodisperse (A). Magnified portion of TEM (B) shows NC of approximately 5 nm in diameter with obvious lattice fringes. Shape and fringing are consistent with zinc blende structure.

This corresponds nicely with the absorption feature at 605 nm (Fig A4), consistent with a nanocrystal of 4.8 nm in diameter, as calculated from previous literature.[37] The nanocrystals exhibit a triangular shape, which is commonly observed with zinc blende nanocrystals. The triangular shape is slightly more pronounced than in normal CdSe nanocrystal reactions, which could result from the different reactivity of the precursors and their binding energies to the different facets.

High resolution EELS analysis is useful for providing elemental analysis on the atomic scale. [66] Manganese is known to have a strong EELS signal, especially when in the oxidation state is +2 and it has a paramagnetic d^5 orbital arrangement.[67] However, this signal may be difficult to detect if the Mn^{2+} is not very concentrated in the nanocrystal. If the

nanocrystal synthesized by the modified Kwak et. al method have the same doping efficiency as the previously reported Mn:CdSe, then the concentration is expected to be quite low at only 4% (at.) or less.[58] When the sample was evaluated using EELS no Mn^{2+} signal was detected, indicating that the sample has very low dopant concentration or possibly no dopant incorporation at all.

A.3.3.3 EPR of Selenium Heavy Synthesis

Another method of investigating the presence and nature of the Mn^{2+} bond in the nanocrystal is measuring the absorption of microwave radiation by unpaired electrons in a strong magnetic field by electron paramagnetic resonance (EPR). The Mn^{2+} ion is paramagnetic, having five unpaired electrons occupying all five d-orbitals, giving a nuclear spin of I=5/2. Splitting patterns are predicted by the equation 2I+1, thus predicting that Mn^{2+} would have a six line pattern, which is indeed a signature of Mn^{2+} hyperfine splitting. The hyperfine splitting reported for Mn^{2+} in bulk CdSe is 62×10-4 cm-1,[70] and the hyperfine splitting for Mn:CdSe nanocrystals was found by Mikulec et. al to be 83×10-4 cm-1.[59] Mikulec conjectures that the larger splitting pattern is a result of the different bonding environments of Mn^{2+} loosely bound to the surface of the nanocrystal instead of in the core.

When the samples were evaluated using EPR (Figure A7), the line shape showed no characteristic hyperfine splitting, indicating no dopant incorporation in the CdSe nanocrystal or surface bound dopant ions.

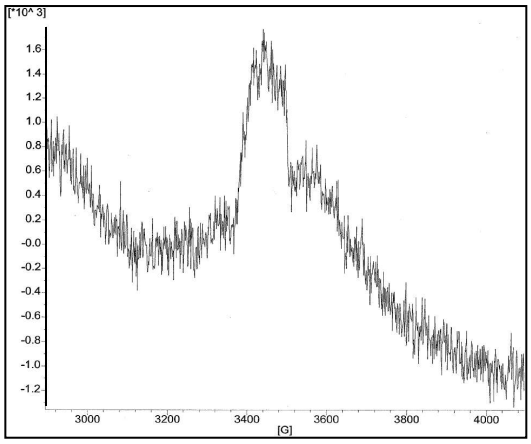

Figure A7. EPR of Se heavy synthesis of Mn:CdSe. No hyperfine splitting is observed.

A.3.3.4 RBS of Selenium Heavy Synthesis: Second Wash Series

The data collected with RBS disagrees with the EELS and EPR data. It is possible that the Mn precursor solubility in the solutions used in the first wash series was too high, so a second wash series was performed on a new batch of nanocrystal subject to the same doping conditions. Six additional extractions with chloroform:acetone were performed after the initial purification. The washed nanocrystals as well as the wash solution were evaluated using RBS (Figure A8). A disappearance of the Mn peak in the nanocrystal samples was observed after only two washes. The wash solution continued to have Mn peaks, indicating no Mn^{2+} was being doped into the CdSe, but that it was all being removed in successive

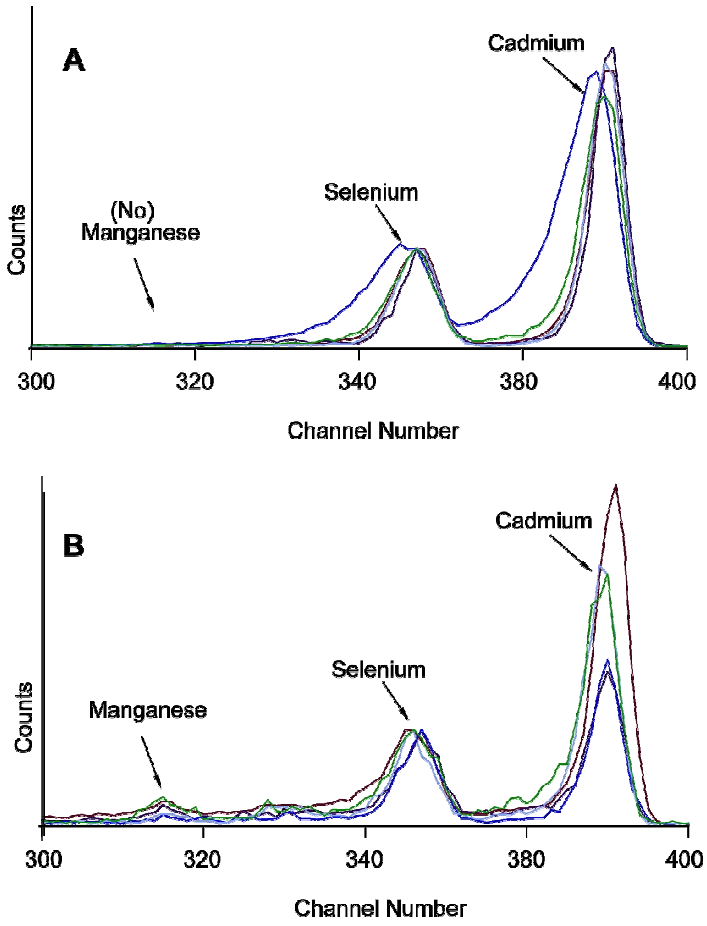

Figure A8. Normalized RBS spectrum, with regards to Se. Nanocrystals subjected to second wash series (A) and the second series wash solutions (B).

washes. These results indicate that the Mn precursor must be more soluble in the chloroform:acetone mixture allowing for better removal of the Mn precursor, and cleaner nanocrystals.

A.4 Conclusion

The selenium heavy modified synthetic method used in this work gave similar results to that reported by Kwak *et al.*, but after further evaluation with RBS, EELS, and EPR were

found to not be successfully doped. Rutherford backscattering spectroscopy is a useful tool for determining nanocrystal stoichiometry, and it sensitive up to a picomole, however it is not able to distinguish between dopant atoms incorporated into nanocrystals and dopant that is in solution with the nanocrystal. EELS and EPR are able to detect nanocrystals doped with paramagnetic manganese as well as reveal the nature of the dopant bond and location. Using these analytical techniques it is concluded that this synthesis was not successful. However, a wash method of additional chloroform:acetone extractions proved more effective than previously reported methods in removing manganese precursor and ions from solution.

A.5 Concluding Remarks

CdSe is a notoriously difficult nanocrystal system to dope with Mn^{2+}. Erwin reported that doping depends on the size, shape, and morphology of the nanocrystals and the surfactants present in solution.[64] Pradhan *et al.* reported that in Mn:ZnSe, the Mn^{2+} precursor should be significantly less reactive than Zn^{2+} if they both have the same carboxylate ligand.[62] Most certainly Cd^{2+} would also be a more reactive precursor. Seemingly, the surfactants present in solution and the shape of the nanocrystal are the varying factors that may make doping in this system difficult. A few more avenues could be explored before abandoning this system. Precursors and surfactants of differing reactivities may provide a more successful approach to this general system. Also, shelling with a more reactive and stable shell, such as ZnS, may allow for the encapsulation of the Mn atoms on the surface of the CdSe nanocrystal that may otherwise be removed during washes.

APPENDIX B

Surface Modifications of Ultrasmall CdSe Nanocrystals

In addition to being able to tune nanocrystal properties by core composition (i.e. alloying and doping), it is also possible to affect photoluminescence by controlling the surface of the particle. Optical studies indicate that surface morphology may play as important a role in photoluminescence as crystallite size, especially in the electronic relaxation processes.[1, 33, 71] Surface studies[33, 42] as well as theoretical modeling [72] agree that the majority of CdSe nanocrystal hole traps originate from surface selenium sp^3-hybridized dangling bond orbitals, leading to charged, higher energy surfaces. Cadmium atoms generally do not act as electron traps because of the superior passivating ability of the surface ligands.[42]

As nanocrystal size decreases entering into the ultrasmall size regime, 1.7 nm and below, the optical properties change dramatically because of the ever increasing surface area to volume ratio. Instead of the size-dependent, strong band edge emission that is typically observed in larger nanocrystals, the ultrasmall CdSe nanocrystals, on the order of 15 Å, are governed by their surface states instead of band gap, producing a white-light emission. [73, 74] This broadband emission covers the wavelengths of the entire visible spectrum, and is characterized by three trap-state emission features (Figure B1) that are size independent.[75]

In order to better understand the nature of the unique, size-independent properties, the surface of the ultrasmall nanocrystals were modified and the effect of the surface change on their optical properties observed. The surface modifications discussed in this appendix are

ligand exchange and shelling, and this work has been published in reports by Dukes[75] and Bowers,[76] respectively.

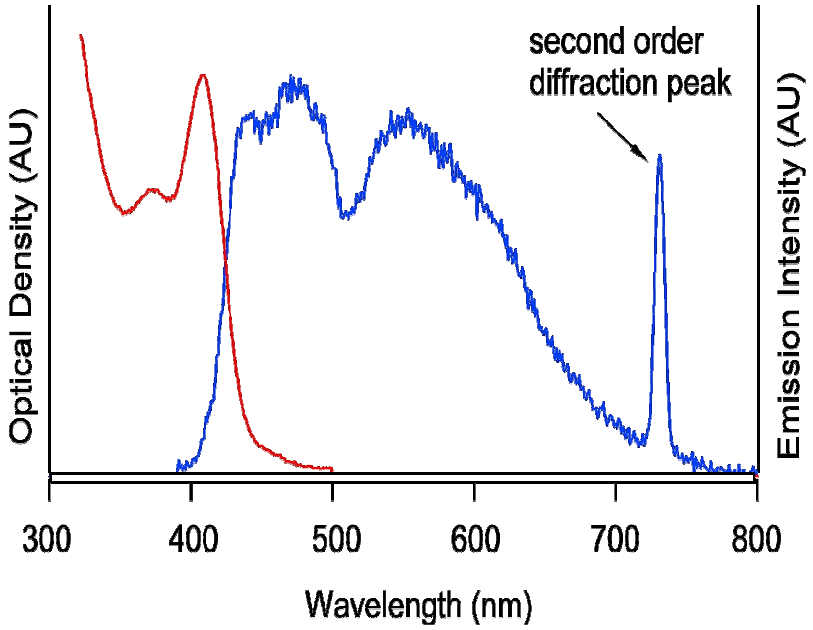

Figure B1. Typical absorption (red) and emission (blue) spectra of ultrasmall white-light emitting nanocrystals.

B.1 Synthesis and Surface Modifications

B.1.1 Ultrasmall CdSe Nanocrystals Synthesis

Tri-*n*-butylphosphine (TBP, tech grade 97-99%), selenium shot (200 mesh), cadmium oxide (Puratrem, 99.999%), hexadecylamine (HDA, tech grade, 90%), triethylphosphite, dodecylbromide, octylbromide, hexadecylbromide, ethyl acetate, hexanes, toluene, methanol, and hexanol (all reagent grade), were purchased from Sigma-Aldrich or Strem if not otherwise indicated and used as delivered. The alkyl phosphonic acids were synthesized by the Michaelis-Arbuzov reaction according to standard procedures.[77, 78] The ultrasmall white-light nanocrystals were synthesized similar to the method reported by Bowers *et al.*[73] The reactive cadmium precursor was prepared by combining 20 g of HDA, 2 mmol of CdO, and 4 mmol of the phosphonic acid in a 100 mL three neck round-bottom flask fitted with a

temperature probe, bump trap, and a rubber septum. The reaction mixture was stirred and purged with argon until the reaction reached 150 °C. The temperature was then raised to 320 °C and stirred until the solution became clear and colorless. Once the solution was colorless, 10 mL of 0.2M Se:TBP solution was injected into the hot solution. A swift injection of 20 mL of butanol (BuOH) was used to halt the reaction at the desired size, cooling the solution to ~130 °C, after which compressed air was used to further cool the solution to 90 °C. Aliquots were taken and diluted with toluene for subsequent characterization. Isolation of the nanocrystals was carried out by precipitation with methanol and collected by centrifugation. The yellow pellet was then dispersed in hexanol and centrifuged to collect the undissolved HDA. The nanocrystals were then precipitated from the hexanol by the addition of methanol, and collected by centrifugation. The cleaned nanocrystals were dispersed in hexanes for characterization, storage, or any other future purpose.

B.1.2 Ligand exchange of Ultrasmall CdSe Nanocrystals

The ultrasmall nanocrystals (already purified) were dispersed in hexanes for ligand exchange. Five milliliters of 0.5 μM nanocrystal solution was added to 15 mL of pure ligand, for ligand exchange with pyridine and oleic acid. These solutions were allowed to stir overnight at room temperature. The nanocrystals were then diluted with hexanes for spectroscopic measurements. For ligand exchange with dodecanethiol, three drops of dodecanethiol were added to a cuvette of ultrasmall nanocrystals in hexanes (0.17 μM) and stirred.

B.1.3 Shelling Ultrasmall CdSe Nanocrystals with ZnS

The ultrasmall nanocrystals were shelled following the procedure reported by Riess *et al.* with modifications.[36] In a three neck flask 10g of TOPO, 10g of HDA, and 0.25g of nanocrystals (already purified) in hexanes were combined and heated under Argon to 150 °C with stirring, distilling off the hexanes. A solution consisting of equal volumes of 0.1M zinc napthonate, 0.1M S:dibutylether, and toluene were mixed in a syringe. The ZnS solution was pumped at a constant rate of 0.78 mL/min into the nanocrystal solution after the completion of distillation, holding the temperature at 150°C for the duration of the shelling. Aliquots were taken before shelling and at regular time intervals for subsequent characterization.

B.1.4 Characterization

Once the ultrasmall nanocrystals had been synthesized and cleaned, and then modified by ligand exchange or shelling, they were characterized to determine size, monodispersity, and photoluminescence. Static absorption (Section 2.3.1) and static emission (Section 2.3.2) were used for the purposes expressed as discussed in the previous sections.

B.2 Results and Discussion

B.2.1 Ligand Exchange of Ultrasmall CdSe Nanocrystals

The white-light emission of ultrasmall nanocrystal is known to result from surface trap site recombination instead of band edge recombination. Nanocrystals in the ultrasmall size regime, 1.7 nm and below, display 3 emission features at 440, 488, and 550 nm. As

noted by Dukes, the bluest peak which appears similar to band edge recombination is "pinned" at 440 nm,[75] ceasing to blue shift as expected in accordance with quantum confinement.[75] Figure B2a illustrates the pinning of the first emissive feature. As the energy of the conduction band becomes greater than that of the surface states, band edge recombination no longer occurs in favor of the lower energy surface state recombination. While the emission of nanocrystals in the ultrasmall regime is pinned, the absorption continues to blue shift. Figure B2b gives an example of the absorption and emission spectra

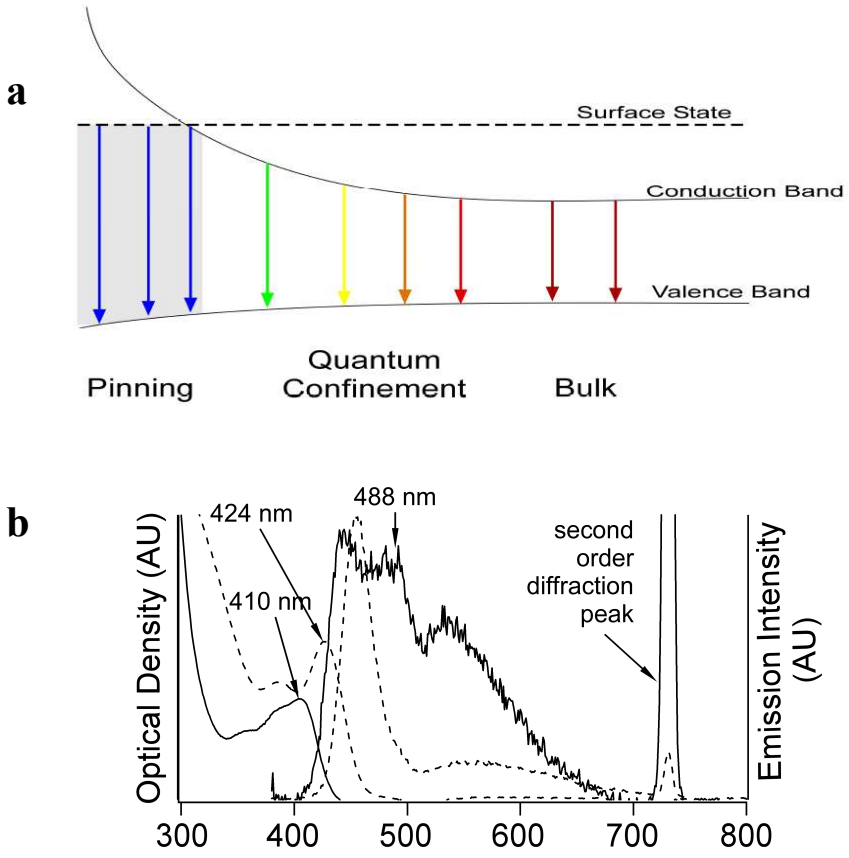

Figure B2. a) Illustration of the pinning behavior of nanocrystals inside of the ultrasmall regime. As the energy of the conduction band rises above that of the surface state, the pinned emission (shaded box) is seen. b) The absorption and emission of nanocrystals within (solid line) and outside (dotted line) the pinning regime.

of a white-light emitting nanocrystal and a slightly larger nanocrystal which exhibits band edge emission.

Recently, theoretical studies have been done to explain the origin of the band gap in ultrasmall nanocrystals. Puzder concluded that surface states created by structural relaxation are responsible for the nanocrystal's emission, [79] while Lee predicts it is a state in the upper conduction band that is unaffected by quantum confinement.[80] Both studies predicted a pinned emission, but neither able to accurately explain the phenomena observed in the white-light emitting ultrasmall nanocrystals.

First feature pinning been seen in broad emitting ultrasmall CdSe nanocrystals, with an absorption below 420 nm. Larger nanocrystals can undergo ligand exchange and while their quantum yield may increase or decrease, the absorption and emission wavelengths are not severely affected because they are not governed by surface states. However, surface modification of ultrasmall nanocrystals allows for investigation into the specific surface states responsible for the broad emission. Several post-preparative ligand exchanges were performed to determine if a different surface passivation, specifically the Cd-ligand bond, would affect the surface state leading to the emission at 440 nm. To modify the surface of the nanocrystals, the ligands must be replaced by exposure to an excess of a competing ligand or capping group.

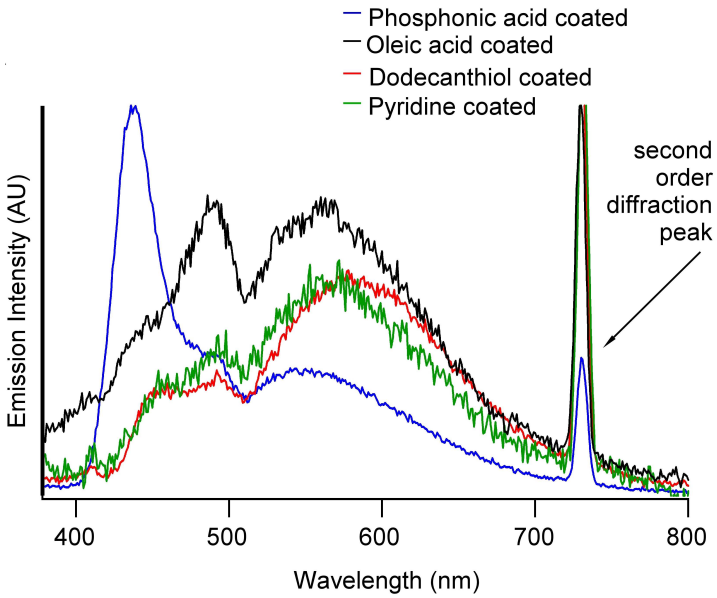

Figure B3. The emission from nanocrystals, 1.6 nm in diameter, synthesized in octylphosphonic acid is shown in blue. After a ligand exchange with dodecane thiol (red), oleic acid (black), and pyridine (green), the emission feature at 440 nm is quenched.

The alkyl phosphonic acid was replaced with dodecanethiol, pyridine, or oleic acid ligands (Figure B3), all of which bind to the surface Cd atoms. In all cases, the emission feature at 440 nm is quenched when a competing ligand replaces the alkyl phosphonic acid, indicating the elimination of the surface state responsible for the emission at 440 nm. The surface state introduced by the phosphonic acid ligand binding to the surface of the nanocrystal is the only state significantly affected by the ligand exchange. The position of the remaining features are preserved, except in the case of the 550 nm emission for dodecanethiol, which undergoes a significant red shift, due to the sulfur atom changing the surface energy.[81] Because the ligand exchange only affects the surface Cd atoms, the retention of the emission at 488 nm may indicate that a Se surface state is responsible for the second emissive feature, as they were unaffected by the ligand exchange. The deep trap emission, caused by surface carrier recombination at dangling bonds of different oxidation

states, also remained mostly unaffected as the surface Se bonds did not participate in ligand exchange.

B.2.2 Shelling Ultrasmall Nanocrystals with ZnS

As discussed in Chapter 1, shelling is a useful surface modification technique for improving the quantum yield of nanocrystals whose emission depends on band edge recombination. In the case of CdSe nanocrystals, which have a band gap of 1.74 eV, ZnS is commonly used because of its wider band gap of 3.6 eV. The inorganic layer of semiconductor material formed around the nanocrystal core passivates surface traps sites and ensures radiative recombination.[24]

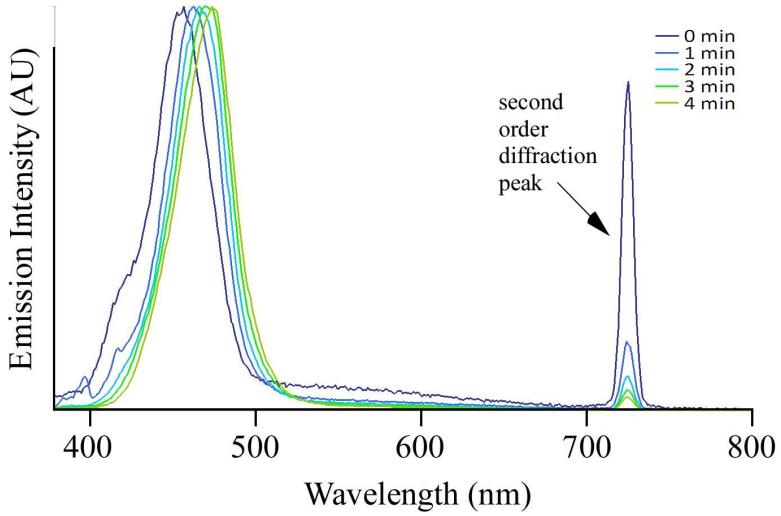

Figure B4. Normalized emission spectra of ultrasmall nanocrystals during ZnS shelling is shown. The broad emissions collapse almost immediately.

Ultrasmall white-light nanocrystals have broad band emission which has been shown to result from the size independent surface states.[75] Because shelling passivates the surface

of the nanocrystal, ultrasmall nanocrystals cannot undergo shelling and still retain their unique white light emissions. Figure B4 shows the significant change that occurs in the emission during shelling, normalized so that the changes to the spectra easily recognizable.

Early in the shelling process, the first "pinned" feature is still visible, although greatly diminished, and the broad emission spectrum collapses almost immediately due to surface passivation. In accordance with the ligand exchange data presented in Section B.2.1, the disappearance of all three features, the first feature corresponding to a state introduced by the Cd-ligand bond, the second feature possibly corresponding to a Se surface state, and deep trap emission from surface trap states created by dangling bonds, indicates that the entire surface of the nanocrystal has been altered and surface state recombination eliminated. This is followed by the appearance of a single, narrow band edge feature. The ZnS shell passivates the core crystallite, eliminating surface traps and allowing for direct radiative recombination resulting in brighter photoluminescence.[24] Although it is not shown in Figure B4, the emergence of band edge emission is accompanied by a large increase in the photoluminescence quantum yield, providing proof of effective shelling. After a certain shell thickness of ZnS, due to defects in the shell producing trap states, or possibly carrier tunneling, the luminescence is quenched. It should be noted that the emission spectra redshift slightly. This behavior has been observed with nanocrystals that are allowed to grow without any shell material, however the redshift is not accompanied by such a dramatic increase in quantum yield.

B.3 Conclusion

Ultrasmall white-light emitting nanocrystals have been shelled with ZnS, a wider band gap material. The shelling layer passivates the surface of the nanocrystal, quenching

the surface states responsible for the unique broadband emission. As the shelling layer thickens, the quantum yield is seen to increase and the emission is governed by band edge recombination. By observing the effect of surface modifications we gain insight into the surface states responsible for the white-light emission of the ultrasmall nanocrystal.

REFERENCES

1. Underwood, D. F.; Kippeny, T.; Rosenthal, S. J., Ultrafast carrier dynamics in CdSe nanocrystals determined by femtosecond fluorescence upconversion spectroscopy. *Journal of Physical Chemistry B* **2001,** 105, (2), 436-443.

2. Brus, L., Electronic Wave-Functions in Semiconductor Clusters - Experiment and Theory. *Journal of Physical Chemistry* **1986,** 90, (12), 2555-2560.

3. Alivisatos, A. P., Semiconductor clusters, nanocrystals, and quantum dots. *Science* **1996,** 271, (5251), 933-937.

4. Colvin, V. L.; Schlamp, M. C.; Alivisatos, A. P., Light-Emitting-Diodes Made from Cadmium Selenide Nanocrystals and a Semiconducting Polymer. *Nature* **1994,** 370, (6488), 354-357.

5. Achermann, M.; Petruska, M. A.; Kos, S.; Smith, D. L.; Koleske, D. D.; Klimov, V. I., Energy-transfer pumping of semiconductor nanocrystals using an epitaxial quantum well. *Nature* **2004,** 429, (6992), 642-646.

6. Firth, A. V.; Cole-Hamilton, D. J.; Allen, J. W., Optical properties of CdSe nanocrystals in a polymer matrix. *Applied Physics Letters* **1999,** 75, (20), 3120-3122.

7. Schreuder, M. A.; Gosnell, J. D.; Smith, N. J.; Warnement, M. R.; Weiss, S. M.; Rosenthal, S. J., Encapsulated white-light CdSe nanocrystals as nanophosphors for solid-state lighting. *Journal of Materials Chemistry* **2008,** 18, (9), 970-975.

8. Greenham, N. C. P., X.G.; Alivisatos, A.P.. , Charge separation and transport in conjugated-polymer/semiconductor-nanocrystal composites studied by photoluminescence quenching and photoconductivity. *Physical Review B* **1996,** 54, (24), 11.

9. Erwin, M. M.; Kadavanich, A. V.; McBride, J.; Kippeny, T.; Pennycook, S.; Rosenthal, S. J., Material characterization of a nanocrystal based photovoltaic device. *European Physical Journal D* **2001,** 16, (1-3), 275-277.

10. Klein, D. L.; Roth, R.; Lim, A. K. L.; Alivisatos, A. P.; McEuen, P. L., A single-electron transistor made from a cadmium selenide nanocrystal. *Nature* **1997,** 389, (6652), 699-701.

11. Alivisatos, A. P., Electrical studies of semiconductor-nanocrystal colloids. *Mrs Bulletin* **1998,** 23, (2), 18-23.

12. Bruchez, M.; Moronne, M.; Gin, P.; Weiss, S.; Alivisatos, A. P., Semiconductor nanocrystals as fluorescent biological labels. *Science* **1998,** 281, (5385), 2013-2016.

13. Warnement, M. R.; Tomlinson, I. D.; Rosenthal, S. J., Fluorescent imaging applications of Quantum Dot probes. *Current Nanoscience* **2007,** 3, (4), 273-284.

14. Rosenthal, S. J.; Tomlinson, A.; Adkins, E. M.; Schroeter, S.; Adams, S.; Swafford, L.; McBride, J.; Wang, Y. Q.; DeFelice, L. J.; Blakely, R. D., Targeting cell surface receptors with ligand-conjugated nanocrystals. *Journal of the American Chemical Society* **2002,** 124, (17), 4586-4594.

15. Swafford, L. A.; Weigand, L. A.; Bowers, M. J.; McBride, J. R.; Rapaport, J. L.; Watt, T. L.; Dixit, S. K.; Feldman, L. C.; Rosenthal, S. J., Homogeneously alloyed CdSxSe1-(x) nanocrystals: Synthesis, characterization, and composition/size-dependent band gap. *Journal of the American Chemical Society* **2006,** 128, (37), 12299-12306.

16. Zimmer, J. P.; Kim, S. W.; Ohnishi, S.; Tanaka, E.; Frangioni, J. V.; Bawendi, M. G., Size series of small indium arsenide-zinc selenide core-shell nanocrystals and their application to in vivo imaging. *Journal of the American Chemical Society* **2006,** 128, (8), 2526-2527.

17. Robel, I.; Subramanian, V.; Kuno, M.; Kamat, P. V., Quantum dot solar cells. Harvesting light energy with CdSe nanocrystals molecularly linked to mesoscopic TiO2 films. *Journal of the American Chemical Society* **2006,** 128, (7), 2385-2393.

18. Zhong, X. H.; Feng, Y. Y.; Knoll, W.; Han, M. Y., Alloyed ZnxCd1-xS nanocrystals with highly narrow luminescence spectral width. *Journal of the American Chemical Society* **2003,** 125, (44), 13559-13563.

19. Zhong, X. H.; Han, M. Y.; Dong, Z. L.; White, T. J.; Knoll, W., Composition-tunable ZnxCd1-xSe nanocrystals with high luminescence and stability. *Journal of the American Chemical Society* **2003,** 125, (28), 8589-8594.

20. Zhong, X. H.; Zhang, Z. H.; Liu, S. H.; Han, M. Y.; Knoll, W., Embryonic nuclei-induced alloying process for the reproducible synthesis of blue-emitting ZnxCd1-xSe nanocrystals with long-time thermal stability in size distribution and emission wavelength. *Journal of Physical Chemistry B* **2004,** 108, (40), 15552-15559.

21. Bailey, R. E.; Nie, S. M., Alloyed semiconductor quantum dots: Tuning the optical properties without changing the particle size. *Journal of the American Chemical Society* **2003,** 125, (23), 7100-7106.

22. Gurusinghe, N. P.; Hewa-Kasakarage, N. N.; Zamkov, M., Composition-tunable properties of CdSxTe1-x alloy nanocrystals. *Journal of Physical Chemistry C* **2008,** 112, (33), 12795-12800.

23. Kuno, M.; Higginson, K. A.; Qadri, S. B.; Yousuf, M.; Lee, S. H.; Davis, B. L.; Mattoussi, H., Molecular clusters of binary and ternary mercury chalcogenides: Colloidal

synthesis, characterization, and optical spectra. *Journal of Physical Chemistry B* **2003,** 107, (24), 5758-5767.

24. Hines, M. A.; Guyot-Sionnest, P., Synthesis and characterization of strongly luminescing ZnS-Capped CdSe nanocrystals. *Journal of Physical Chemistry* **1996,** 100, (2), 468-471.

25. Kippeny, T.; Swafford, L. A.; Rosenthal, S. J., Semiconductor nanocrystals: A powerful visual aid for introducing the particle in a box. *Journal of Chemical Education* **2002,** 79, (9), 1094-1100.

26. Brus, L. E., Electron Electron and Electron-Hole Interactions in Small Semiconductor Crystallites - the Size Dependence of the Lowest Excited Electronic State. *Journal of Chemical Physics* **1984,** 80, (9), 4403-4409.

27. Murray, C. B.; Norris, D. J.; Bawendi, M. G., Synthesis and Characterization of Nearly Monodisperse Cde (E = S, Se, Te) Semiconductor Nanocrystallites. *Journal of the American Chemical Society* **1993,** 115, (19), 8706-8715.

28. McBride, J.; Treadway, J.; Feldman, L. C.; Pennycook, S. J.; Rosenthal, S. J., Structural basis for near unity quantum yield core/shell nanostructures. *Nano Letters* **2006,** 6, (7), 1496-1501.

29. Bernard, J. E.; Zunger, A., Electronic-Structure of Zns, Znse, Znte, and Their Pseudobinary Alloys. *Physical Review B* **1987,** 36, (6), 3199-3228.

30. Vegard, L., *Zeitschrift fur Physik*
1921, 5, 17-26.

31. Garrett, M. D.; Dukes, A. D.; McBride, J. R.; Smith, N. J.; Pennycook, S. J.; Rosenthal, S. J., Band edge recombination in CdSe, CdS and CdSxSe1-x alloy nanocrystals observed by ultrafast fluorescence upconversion: The effect of surface trap states. *Journal of Physical Chemistry C* **2008,** 112, (33), 12736-12746.

32. Peng, X. G.; Wickham, J.; Alivisatos, A. P., Kinetics of II-VI and III-V colloidal semiconductor nanocrystal growth: "Focusing" of size distributions. *Journal of the American Chemical Society* **1998,** 120, (21), 5343-5344.

33. Katari, J. E. B.; Colvin, V. L.; Alivisatos, A. P., X-Ray Photoelectron-Spectroscopy of Cdse Nanocrystals with Applications to Studies of the Nanocrystal Surface. *Journal of Physical Chemistry* **1994,** 98, (15), 4109-4117.

34. Yu, W. W.; Peng, X. G., Formation of high-quality CdS and other II-VI semiconductor nanocrystals in noncoordinating solvents: Tunable reactivity of monomers. *Angewandte Chemie-International Edition* **2002,** 41, (13), 2368-2371.

35. Qu, L. H.; Peng, X. G., Control of photoluminescence properties of CdSe nanocrystals in growth. *Journal of the American Chemical Society* **2002,** 124, (9), 2049-2055.

36. Reiss, P.; Carayon, S.; Bleuse, J.; Pron, A., Low polydispersity core/shell nanocrystals of CdSe/ZnSe and CdSe/ZnSe/ZnS type: preparation and optical studies. *Synthetic Metals* **2003,** 139, (3), 649-652.

37. Yu, W. W.; Qu, L. H.; Guo, W. Z.; Peng, X. G., Experimental determination of the extinction coefficient of CdTe, CdSe, and CdS nanocrystals. *Chemistry of Materials* **2003,** 15, (14), 2854-2860.

38. Klimov, V. I.; McBranch, D. W.; Leatherdale, C. A.; Bawendi, M. G., Electron and hole relaxation pathways in semiconductor quantum dots. *Physical Review B* **1999,** 60, (19), 13740-13749.

39. McBride, J. R. Atomic Level Characterization of CdSe Nanocrystal Systems using Atomic Number Contrast Scanning and Transmission Electron Microscopy and Rutherford Backscattering Spectroscopy. Vanderbilt University, Nashville, 2005.

40. Rosenthal, S. J.; McBride, J.; Pennycook, S. J.; Feldman, L. C., Synthesis, surface studies, composition and structural characterization of CdSe, core/shell and biologically active nanocrystals. *Surface Science Reports* **2007,** 62, (4), 111-157.

41. Swafford, L. A. Homogeneously Alloyed Cadmium Sulfoselenide Nanocrystals. Vanderbilt University, Nashville, 2006.

42. Taylor, J.; Kippeny, T.; Rosenthal, S. J., Surface stoichiometry of CdSe nanocrystals determined by Rutherford backscattering spectroscopy. *Journal of Cluster Science* **2001,** 12, (4), 571-582.

43. Feldman, L. C.; Mayer, J. W., North Holland-Elsevier: New York, 1986.

44. Garrett, M. D.; Bowers, M. J.; McBride, J. R.; Orndorff, R. L.; Pennycook, S. J.; Rosenthal, S. J., Band edge dynamics in CdSe nanocrystals observed by ultrafast fluorescence upconversion. *Journal of Physical Chemistry C* **2008,** 112, (2), 436-442.

45. *Semiconductors, Data in Science and Technology*. Springer-Verlag: Berlin, 1992.

46. Dabbousi, B. O.; RodriguezViejo, J.; Mikulec, F. V.; Heine, J. R.; Mattoussi, H.; Ober, R.; Jensen, K. F.; Bawendi, M. G., (CdSe)ZnS core-shell quantum dots: Synthesis and characterization of a size series of highly luminescent nanocrystallites. *Journal of Physical Chemistry B* **1997,** 101, (46), 9463-9475.

47. Furdyna, J. K., Diluted Magnetic Semiconductors. *Journal of Applied Physics* **1988,** 64, (4), R29-R64.

48. Sapra, S.; Prakash, A.; Ghangrekar, A.; Periasamy, N.; Sarma, D. D., Emission properties of manganese-doped ZnS nanocrystals. *Journal of Physical Chemistry B* **2005,** 109, (5), 1663-1668.

49. Nag, A.; Sapra, S.; Nagamani, C.; Sharma, A.; Pradhan, N.; Bhat, S. V.; Sarma, D. D., A study of Mn2+ doping in CdS nanocrystals. *Chemistry of Materials* **2007,** 19, (13), 3252-3259.

50. Ohno, H., Making nonmagnetic semiconductors ferromagnetic. *Science* **1998,** 281, (5379), 951-956.

51. Das Sarma, S., Spintronics. *American Scientist* **2001,** 89, (6), 516-523.

52. Nag, A.; Chakraborty, S.; Sarma, D. D., To Dope Mn^{+2} in a Semiconducting Nanocrystal. *Journal of the American Chemical Society* **2008,** 130, (32), 6.

53. Norris, D. J.; Yao, N.; Charnock, F. T.; Kennedy, T. A., High-quality manganese-doped ZnSe nanocrystals. *Nano Letters* **2001,** 1, (1), 3-7.

54. Li, Y. Q.; Zapien, J. A.; Shan, Y. Y.; Liu, Y. K.; Lee, S. T., Manganese doping and optical properties of ZnS nanoribbons by postannealing. *Applied Physics Letters* **2006,** 88, (1), 3.

55. Archer, P. I.; Santangelo, S. A.; Gamelin, D. R., Inorganic cluster syntheses of TM2+-doped quantum dots (CdSe, CdS, CdSe/CdS): Physical property dependence on dopant locale. *Journal of the American Chemical Society* **2007,** 129, (31), 9808-9818.

56. Artemyev, M. V.; Gurinovich, L. I.; Stupak, A. P.; Gaponenko, S. V. In *Luminescence of CdS nanoparticles doped with Mn*, 2001; Wiley-V C H Verlag Gmbh: 2001; pp 191-194.

57. Bhargava, R. N.; Gallagher, D.; Hong, X.; Nurmikko, A., Optical-Properties of Manganese-Doped Nanocrystals of Zns. *Physical Review Letters* **1994,** 72, (3), 416-419.

58. Kwak, W. C.; Sung, Y. M.; Kim, T. G.; Chae, W. S., Synthesis of Mn-doped zinc blende CdSe nanocrystals. *Applied Physics Letters* **2007,** 90, (17), 2.

59. Mikulec, F. V.; Kuno, M.; Bennati, M.; Hall, D. A.; Griffin, R. G.; Bawendi, M. G., Organometallic synthesis and spectroscopic characterization of manganese-doped CdSe nanocrystals. *Journal of the American Chemical Society* **2000,** 122, (11), 2532-2540.

60. Cumberland, S. L.; Hanif, K. M.; Javier, A.; Khitrov, G. A.; Strouse, G. F.; Woessner, S. M.; Yun, C. S., Inorganic clusters as single-source precursors for preparation of CdSe, ZnSe, and CdSe/ZnS nanomaterials. *Chemistry of Materials* **2002,** 14, (4), 1576-1584.

61. Tang, X.; Urbaszek, B.; Graham, T. C. M.; Warburton, R. J.; Prior, K. A.; Cavenett, B. C. In *Growth and characterization of CdSe : Mn quantum dots*, 2003; Elsevier Science Bv: 2003; pp 586-590.

62. Pradhan, N.; Goorskey, D.; Thessing, J.; Peng, X. G., An alternative of CdSe nanocrystal emitters: Pure and tunable impurity emissions in ZnSe nanocrystals. *Journal of the American Chemical Society* **2005,** 127, (50), 17586-17587.

63. Dalpian, G. M.; da Silva, A. J. R.; Fazzio, A. In *Adsorption of Mn atoms on the Si(100) surface*, 2004; Elsevier Science Bv: 2004; pp 688-692.

64. Norris, D. J.; Efros, A. L.; Erwin, S. C., Doped nanocrystals. *Science* **2008,** 319, (5871), 1776-1779.

65. Erwin, S. C.; Zu, L. J.; Haftel, M. I.; Efros, A. L.; Kennedy, T. A.; Norris, D. J., Doping semiconductor nanocrystals. *Nature* **2005,** 436, (7047), 91-94.

66. Kadavanich, A. V.; Kippeny, T. C.; Erwin, M. M.; Pennycook, S. J.; Rosenthal, S. J., Sublattice Resolution Structural and Chemical Analysis of Individual CdSe Nanocrystals Using Atomic Number Contrast Scanning Transmission Electron Microscopy and Electron Energy Loss Spectroscopy. *Journal of Physical Chemistry B* **2001,** 105, 9.

67. Sparrow, T. G.; Williams, B. G.; Rao, C. N. R.; Thomas, J. M., L_3/L_2 White-Line Intensity Ratios in the Electron Energy-Loss Spectra of 3d Transition Metal Oxides. *Chemical Physics Letters* **1984,** 108, (6), 4.

68. Kennedy, T. A.; Glaser, E. R.; Klein, P. B.; Bhargava, R. N., Symmetry and Electronic-Structure of the Mn Impurity in Zns Nanocrystals. *Physical Review B* **1995,** 52, (20), 14356-14359.

69. Beaulac, R.; Archer, P. I.; Liu, X. Y.; Lee, S.; Salley, G. M.; Dobrowolska, M.; Furdyna, J. K.; Gamelin, D. R., Spin-polarizable excitonic luminescence in colloidal Mn2+-doped CdSe quantum dots. *Nano Letters* **2008,** 8, (4), 1197-1201.

70. Ludwig, G. W.; Woodbury, H. H., *In Solid State Physics*. Academic Press: New York, 1962; Vol. 13, p p297.

71. Becerra, L. R.; Murray, C. B.; Griffin, R. G.; Bawendi, M. G., Investigation of the Surface-Morphology of Capped Cdse Nanocrystallites by P-31 Nuclear-Magnetic-Resonance. *Journal of Chemical Physics* **1994,** 100, (4), 3297-3300.

72. Leung, K.; Whaley, K. B., Surface relaxation in CdSe nanocrystals. *Journal of Chemical Physics* **1999,** 110, (22), 11012-11022.

73. Bowers, M. J.; McBride, J. R.; Rosenthal, S. J., White-light emission from magic-sized cadmium selenide nanocrystals. *Journal of the American Chemical Society* **2005,** 127, (44), 15378-15379.

74. http://hyperphysics.phy-astr.gsu.edu/hbase/vision/cie.html#c2

75. Dukes, A. D. I.; Schreuder, M. A.; Sammons, J. A.; McBride, J. R.; Smith, N. J.; Rosenthal, S. J., Pinned emission from ultrasmall cadmium selenide nanocrystals. *The Journal of Chemical Physics* **2008,** 129.

76. Bowers, M. J. I.; McBride, J. R.; Garrett, M. D.; Sammons, J. A.; Dukes, A. D. I.; Schreuder, M. A.; Watt, T. L.; Lupini, A. R.; Pennycook, S. J.; Rosenthal, S. J., Structure and Ultrafast Dynamics of White-Light-Emitting CdSe Nanocrystals. *Journal of the American Chemical Society* **2009,** 131, 5730-5731.

77. Smith, M. B., *Organic Synthesis*. John Wiley and Sons, Inc.: 1994.

78. Smith, M. B.; March, J., *March's Advanced Organic Chemistry: reactions, mechanisms, and structure*. 5th ed.; John Wiley and Sons, Inc.: New York, 2001.

79. Puzder, A.; Williamson, A. J.; Gygi, F.; Galli, G., Self-healing of CdSe nanocrystals: First-principles calculations. *Physical Review Letters* **2004,** 92, (21), 4.

80. Lee, J. R. I.; Meulenberg, R. W.; Hanif, K. M.; Mattoussi, H.; Klepeis, J. E.; Terminello, L. J.; van Buuren, T., Experimental observation of quantum confinement in the conduction band of CdSe quantum dots. *Physical Review Letters* **2007,** 98, (14), 4.

81. Munro, A. M.; Plante, I. J. L.; Ng, M. S.; Ginger, D. S., Quantitative study of the effects of surface ligand concentration on CdSe nanocrystal photoluminescence. *Journal of Physical Chemistry C* **2007,** 111, (17), 6220-6227.